8
Special Catalytic Systems

8.1
Electrocatalysis

8.1.1
Fundamentals of Electrocatalysis

Katharina Krischer and Elena R. Savinova*

8.1.1.1 **Introduction**

Electrochemical reactions are reactions in which a charge transfer across the interface between electrode and electrolyte takes place. If the electrode acts as a heterogeneous catalyst, i.e. if it accelerates the reaction, the phenomenon is addressed as electrocatalysis. This occurs primarily when reaction educts, products or intermediates adsorb at the electrode surface. Hence electrocatalysis and heterogeneous catalysis are closely related phenomena, the difference resulting from the net charge transfer in electrochemical reactions. The latter causes the reaction rate to depend on the electrostatic potential drop which develops in the interfacial region between the electrode and the electrolyte. This adds an additional and readily controllable parameter – the electrode potential – as a means to influence electrocatalytic processes, accelerating desired reactions and suppressing unwanted ones. Note that a shift of the electrostatic potential of an electrode by 1 V is equivalent to a change of the free energy by nearly 100 kJ mol^{-1}. Hence whereas in heterogeneous catalysis reaction temperature is used as the means to influence reaction rates and shift the thermodynamic equilibrium, in electrocatalysis the electrode potential partially takes this role.

A further complication in electrocatalysis is that the electrode potential not only influences the activation energies of electrocatalytic reactions by shifting electronic energies in the electrode, but also affects the structure of the interfacial region, which in turn affects the rate of interfacial processes. Especially drastic changes of the reaction rate may be observed if a variation of the electrode potential changes the state of the electrode surface.

Electrocatalysis developed at the interface of electrochemistry and heterogeneous catalysis, the latter often serving as its conceptual base. During recent decades, both fields have merged closer together in a need to address new technological and fundamental challenges. Their proximity manifests itself in the most evident way in the so-called NEMCA effect (non-Faradaic electrochemical modification of catalysis). It denotes an electrochemical promotion of catalysis and demonstrates that the interfacial potential drop may also influence the rates of catalytic (no net charge transfer) reactions (see Chapter 8.1.2).

Electrochemical reactions always involve a conversion of chemical into electrical energy or of electrical into chemical energy. The first type of reaction takes place in batteries and fuel cells and the second in the production or decontamination of chemicals. To optimize these processes in terms of energy (power) production and consumption, respectively, is the main goal of industrial electrocatalysis. Concerning fuel cells (FCs), electrocatalysis comes into play in all types of FCs, i.e. in high-temperature solid oxide fuel cells (SOFCs), medium-temperature molten carbonate fuel cells (MCFCs) and low-temperature FCs, such as the alkaline and the polymer electrolyte (PEMFC) fuel cell [1]. Each type of FC has its niche application for delivering stationary, mobile or portable power. Hydrogen is the most important fuel, the evolution/oxidation of hydrogen also being the prototype electrocatalytic reaction with which many concepts of electrocatalysis were developed. In addition, research efforts are aimed towards the direct oxidation of hydrocarbons in high-temperature SOFCs [1, 2] and alcohols in low-temperature direct alcohol fuel cells (DAFCs [1, 3–6]). Oxygen is the most accessible oxidant, hence oxygen reduction serves as the cathode reaction in all types of fuel cells. The reduction of oxygen is a very sluggish reaction and it is very sensitive to the electrode material. This renders oxygen reduction

References see page 1902

---

* Corresponding author.

Handbook of Heterogeneous Catalysis, 2nd Ed.
Edited by G. Ertl, H. Knözinger, F. Schüth, and J. Weitkamp

ISBN: 978-3-527-31241-2

one of the most important topics in current electrocatalysis research. In electrosynthesis, the most important catalyzed reactions are water electrolysis [7, 8], chlorine production [7, 8], hydrogen peroxide production, electrocatalytic hydrogenation reactions [9] and electrochemical reduction of CO_2 [10].

Fundamental research in electrocatalysis is aimed primarily at understanding which properties of the electrode determine its reactivity. For decades electrochemistry and electrocatalysis remained basically empirical disciplines. This has drastically changed, however, in the last three decades with the emergence of electrochemical surface science [11–13] owing to the advances in (i) the preparation of well-defined single-crystal electrodes, (ii) the introduction of UHV-based [14] and especially *in situ* methods of surface characterization [15] (including vibrational spectroscopy [16–18], X-ray absorption spectroscopy [19] and scattering [20], scanning probe microscopy [21–23], second harmonic generation [24], electrochemical NMR [25, 26], the electrochemical quartz crystal microbalance [27] and differential electrochemical mass spectrometry [28]) and (iii) *ab initio* quantum mechanical approaches to the description of the structure of the double layer [29–31] and the kinetics of charge transfer reactions [32–34].

In this chapter, first the basic principles of electrocatalysis are reviewed, that is, the structure of the electrode/electrolyte interface and the driving force for charge transfer at electrodes (Section 8.1.1.2), the main kinetic parameters and their relationship to mechanisms (Section 8.1.1.3) and basic concepts of electrocatalysis. The latter have much in common with heterogeneous catalysis. However, it is elaborated in detail since there are many misinterpretations concerning relationships between catalytic activity and properties of the electrocatalytic reaction in the electrochemical literature. In Sections 8.1.1.4 and 8.1.1.5, we consider the electrocatalytic reactions occurring at the hydrogen electrode (hydrogen evolution and oxidation) and the oxygen electrode (oxygen evolution and reduction) in some detail. These reactions are outstanding because of their importance for both the development of fundamental concepts and their technological importance. Treatments of other electrocatalytic reactions, such as CO oxidation, methanol oxidation and carbon dioxide reduction, can be found in more specialized books and review articles [1, 35].

8.1.1.2 The Electrical Double Layer and Potentials

Electrochemical reactions occur at the interface between an electronic and an ionic conductor. Instances of some practical relevance include solid/liquid, solid/polymer and solid/solid interfaces. The electrical and chemical properties of the interface determine the rate of an electrochemical reaction. They are intimately related to the presence of an electric field across the interface. This section reviews the properties of the solid/liquid interface. Section 8.1.1.2.1 deals with the structure of the interfacial region, the so-called electrical double layer. In Section 8.1.1.2.2, important concepts such as electrode potential, work function of an electrode and potential of zero charge are introduced. Potential distributions in galvanic and electrolytic electrochemical cells are discussed in Section 8.1.1.2.3. These considerations naturally lead to the definition of the overpotential, the basic quantity for any treatment of the rate of an electrochemical reaction, which is addressed in Sections 8.1.1.3 and 8.1.1.4.

Many of the concepts developed in this section for the solid/liquid interface apply qualitatively also to other types of interfaces. For particular properties of the solid/solid or solid/gas interfaces we refer the reader to Ref. [36], solid/polymer interfaces are treated in Ref. [37] and aspects of semiconductor electrochemistry are considered in, e.g., Ref. [38].

8.1.1.2.1 The Electrical Double Layer

If a metal electrode is brought into contact with an electrolyte, an interfacial region establishes with excess charge carriers of opposite sign on the solution and the electrode sides. The region in which the free charge accumulates is called the electrical double layer (DL). On the electrode surface, the charge, i.e. an excess or deficiency of electrons, resides in a thin layer of less than 0.1 Å [39]. It is counterbalanced by cations or anions of the electrolyte that accumulate in front of the electrode, primarily owing to Coulomb forces. In addition, the ions might also interact chemically with the electrode surface such that the detailed distribution of the excess ions in the interfacial region depends not only on the charge density on the electrode and the conductivity of the electrolyte but also on the chemical nature of the electrode and electrolyte. However, in all cases the counter ions tend to form a layered structure (Fig. 1). The layer closest to the electrode surface is formed by ions exhibiting a strong chemical interaction with the electrode material. These are mainly polarizable anions that tend to shed part of their water (solvent) shell to adsorb directly at the electrode surface and they may do so to some extent even if the surface carries the same charge as the adsorbing ions. For the simple case of monatomic ions (e.g. halide anions), the center of charge of these chemisorbed ions coincides approximately with the radius of the adsorbing species and the plane going through it is called the inner Helmholtz plane (IHP). Ions that are attracted only electrostatically to the electrode surface keep their

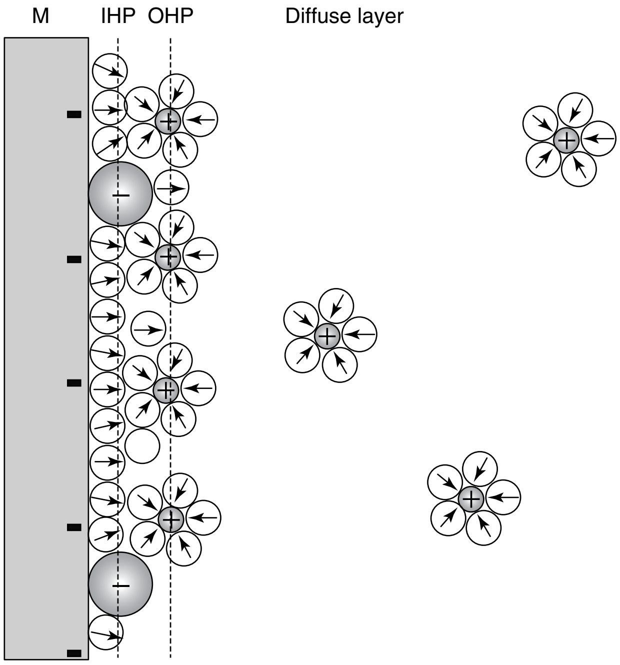

Fig. 1 Model of the electrical double layer. M, metal electrode. IHP: inner Helmholtz plane. OHP: outer Helmholtz plane.

hydration shell and thus may approach the electrode at most up to a distance that corresponds to the radius of the hydrated ion. The center of charge of this layer of closest approach is called the outer Helmholtz plane (OHP) and the corresponding part of the DL is usually termed the compact layer. Counteracting the electrostatic force acting on the ions towards the electrode is an entropic force that entails a continuous decay of the concentration of the excess ions to the bulk value with increasing distance from the electrode. This part of the DL is called diffuse DL; its extension depends on the conductivity of the electrolyte. It can be neglected for concentrated solutions ($\sim$1 M) and reaches up to several tens of nanometers for dilute electrolytes ($\leq 10^{-3}$ M).

In concentrated electrolytes, the electrical DL behaves similar to a capacitor whereby the metal surface and the OHP take on the role of the capacitor plates. Thus, the DL can be charged or discharged by changing the electric potential of the electrode with respect to the one of the electrolyte, whereby the total charge on the electrode, $|q^{\mathrm{m}}|$, is always equal in magnitude to the total charge of the ions on the solution side, $|q^{\mathrm{s}}|$. In other words, if A is the electrode area in contact with the electrolyte and $\sigma^{\mathrm{m(s)}} = q^{\mathrm{m(s)}}/A$ are the respective charge densities, $\sigma^{\mathrm{m}} = -\sigma^{\mathrm{s}}$. In dilute electrolytes the total DL capacitance C is given by

$$\frac{1}{C} = \frac{1}{C^{\mathrm{H}}} + \frac{1}{C^{\mathrm{d}}} \tag{1}$$

where C^{H} and C^{d} are the capacitances related to the OHP and the diffuse DL, respectively. In aqueous electrolytes, the gap between the electrode and the OHP is filled by water molecules that have a permanent dipole moment and thus a high dielectric constant. Although the latter is drastically decreased within the DL compared to the value of bulk water, ensuing from the partially frozen degrees of motion, the dielectric constant is comparably high. Together with the microscopic distance between the plates, the capacitance of the DL is typically in the range 10–40 μF cm^{-2} and is thus much higher than that of usual electronic capacitive devices. Another important difference from the latter is that the DL capacitance depends on the voltage drop across the DL. An extensive treatment of the differential capacitance of electrodes can be found in Ref. [40].

The picture of the electrical DL we have given above was successively developed and refined by Helmholtz, Gouy–Chapman, Stern and Graham. The corresponding electric potential profile across the DL is in the absence of specific adsorption characterized by a linear drop between the electrode and the OHP and a monotonic, non-linear decay across the diffuse layer, which approaches an exponential decay for small charge densities on the electrode (or voltage drops across the DL not larger than a few tens of millivolts) (Fig. 2a). Chemisorbed ions may drastically alter the potential profile (Fig 2b). Thus, the potential profile across the DL can differ significantly for different electrode materials even when in contact with the same electrolyte and for identical electrode potential (see also Section 8.1.1.2.2). Therefore, the electrostatic potential in the reaction plane, i.e. the location from which the reacting species exchange ions or electrons with the electrode, also varies in general with the electrode material and with it the reaction rate. In this respect, the DL structure is an important aspect of electrocatalysis. We will come back to this point in Section 8.1.1.4.2.

8.1.1.2.2 The Work Function of an Electrode, the Electrode Potential and the Potential of Zero Charge

The energy of a charged particle i in a bulk phase α is equal to the electrochemical potential of particle i in phase α, $\tilde{\mu}_i^{\alpha}$ [41]:

$$\tilde{\mu}_i^{\alpha} = \mu_i^{\alpha} + ze\phi^{\alpha} \tag{2}$$

where μ_i^{α} is the chemical potential of particle i in phase α, z and ze are its charge number and total charge, respectively, and ϕ^{α} the electrostatic potential in the bulk phase α. Defining the zero energy of the particle as its energy in a vacuum at infinity, the electrochemical potential is equal to the work required to bring particle i from infinity into the bulk phase. The electrostatic

References see page 1902

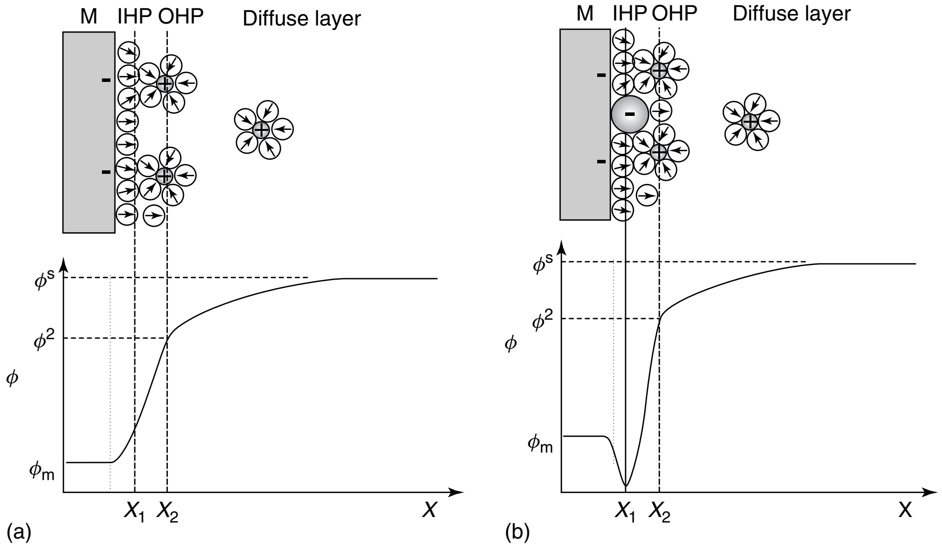

Fig. 2 Potential profiles across the electrical double layer in the absence (a) and presence (b) of specific adsorption.

potential ϕ^α is composed of two contributions, the electrostatic outer or Volta potential, ψ^α, and the surface potential of the phase α, χ^α:

$$\phi^\alpha = \chi^\alpha + \psi^\alpha \tag{3}$$

ψ^α results from excess charge carriers in phase α, which induce in the surroundings an electric field. It is defined through the work required to bring a unit charge from infinity to a locus close the surface, where ψ has already its maximum value but chemical interactions or image forces do not yet have a noticeable effect. The origin of χ^α is a dipole layer at the surface. It might ensue from a monolayer of adsorbed, oriented dipoles but it also exists in the absence of any adsorbates, in which case it is due to asymmetric forces acting on the surface atoms or molecules building up the phase; χ^α thus depends on the geometric arrangement of the atomic/molecular constituents and is different for different crystallographic orientations.

According to Eqs. (2) and (3), the energy required to add a particle to the uncharged phase is given by

$$\alpha_i^\alpha = \mu_i^\alpha + z_i e \chi^\alpha \tag{4}$$

The quantity α is called the real potential; α can also be interpreted as the energy required to transfer the particle from a point in front of the surface (which is in contact with a vacuum) across the dipole layer. For a metal phase and electrons, $-\alpha$ is identical with the electron work function, Φ^m:

$$\alpha_e^m = -\Phi^m \tag{5}$$

Since χ^α depends on the crystallographic orientation, so does the work function, which increases with the density of atoms on the surface. Below we will discuss that there is a correlation between the work function of a metal electrode and properties characterizing its electrocatalytic activity.

The driving force for the formation of the electrical potential drop across the electrode/electrolyte interface, $\Delta\phi$, is a gradient in the electrochemical potential of charged species i that can cross the phase boundary. For example, in the case of a Pt electrode in contact with an acidic electrolyte, protons from the electrolyte can adsorb at the electrode and will do so until their energy in both phases is equal. Thus, under equilibrium conditions, the electrochemical potentials of hydrogen adatoms on the Pt surface and protons in the electrolyte are equal or, more generally, the electrochemical potentials of species i in both phases adjust:

$$\tilde{\mu}_i^m = \tilde{\mu}_i^s \tag{6}$$

where the superscripts m and s denote the metal (electrode) and solution (electrolyte) phases, respectively.

Combining Eqs. (2) and (6), it follows that the potential drop across the DL is determined by the difference in the chemical potentials of the species in the two phases:

$$\Delta\phi = \phi^m - \phi^s = \frac{\mu_i^s - \mu_i^m}{ze} \tag{7}$$

$\Delta\phi$ is of great importance for electrode reactions, yet it is not accessible in an experiment: Any measurement involves two electrodes, which will in general be of different materials. In this case, there are at least three

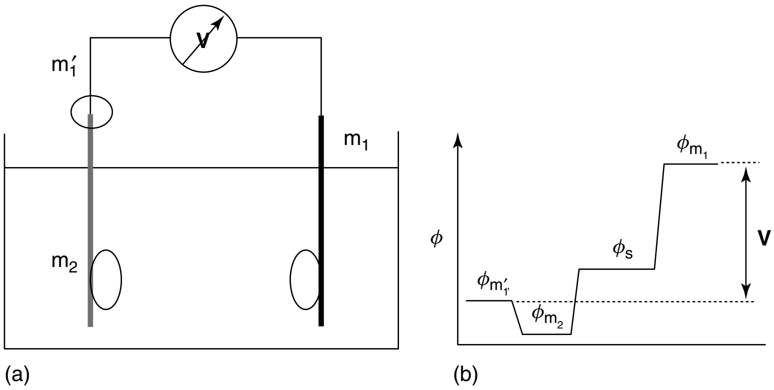

Fig. 3 (a) Schematics of an electrochemical cell with the interfaces at which potential drops establish encircled. (b) Potential drops that contribute to the measured voltage V in an electrochemical cell.

interfaces that determine the measured voltage: two electrode/solution interfaces and a metal/metal interface (Fig. 3). The electrochemical potentials at the metal/metal interface adjust and hence

$$\begin{aligned}\tilde{\mu}_e^{m_1'} &= \mu_e^{m_1} - e\phi^{m_1'} \\ &= \mu_e^{m_2} - e\phi^{m_2} = \tilde{\mu}_e^{m_2}\end{aligned} \tag{8}$$

Here the two metals are denoted by m_1 and m_2 and m_1' refers to the m_1 metal in contact with m_2, whose electrostatic potential will in general be different from that of m_1 at the other pole. The measured voltage V is thus the sum of the potential drops at the three interfaces (Fig. 3b):

$$\begin{aligned}V &= (\phi^{m_1} - \phi^{s}) + (\phi^{s} - \phi^{m_2}) + (\phi^{m_2} - \phi^{m_1'}) \\ &= \Delta\phi_{m_1} - \Delta\phi_{m_2} + (\phi^{m_2} - \phi^{m_1'})\end{aligned} \tag{9}$$

Using Eq. (8), we can express the potential drop across the metal/metal interface in terms of the chemical potentials of an electron in the two metals:

$$\begin{aligned}V &= \Delta\phi_{m_1} - \Delta\phi_{m_2} + \frac{\mu_e^{m_1}}{e} - \frac{\mu_e^{m_2}}{e} \\ &= \left(\Delta\phi_{m_1} + \frac{\mu_e^{m_1}}{e}\right) - \left(\Delta\phi_{m_2} + \frac{\mu_e^{m_2}}{e}\right) \\ &\equiv E_1 - E_2\end{aligned} \tag{10}$$

where E is defined as the electrode potential. Thus, in contrast to statements in some textbooks, the electrode potential is not equal to the interfacial potential drop. Since the absolute value of the electrode potential is also not accessible through any measurement, the values reported in the literature always correspond to the differences between two electrode potentials: the sought one and a reference electrode. In order to be able to compare different electrode potentials, the electrode potential of the standard hydrogen electrode (SHE), i.e. an electrode in a solution of unit activity of protons in equilibrium with H_2 gas at fugacity 1, has been arbitrarily chosen as zero of the electrode potential scale, $E_{SHE} = 0$. For tabulated electrode potentials it is implicitly assumed that the potential of the electrode of interest is measured against an SHE. The concentration dependence of E vs. SHE is given by the well-known Nernst equation, which for the simple redox reaction $O + ne \rightleftharpoons R$ reads

$$E = E^0 + \frac{RT}{nF}\ln\left(\frac{a_O}{a_R}\right) \tag{11}$$

where $a_{O(R)}$ denotes the activities of the oxidized (reduced) species and n the number of electrons transferred. E^0 is the standard electrode potential, i.e. the electrode potential when all substances are at unit activity.

Since the electrode potential depends on the chemical potential of electrons in the metal electrode, the interfacial potential drop $\Delta\phi$ differs for different materials, even at equal electrode potential. For example, an Ir and a Pt electrode in contact with an electrolyte of unit activity of protons and H_2 gas of unit fugacity both have an equilibrium electrode potential of zero, $E^{Ir} = E^{Pt} = 0$, but obviously $\mu_e^{Ir} \neq \mu_e^{Pt}$ and therefore $\Delta\phi^{Ir} \neq \Delta\phi^{Pt}$. This means that the rate of an electrochemical reaction and also its mechanism may to a certain extent depend on the electrode material even in the absence of adsorption of reactants or intermediates, a factor that is important for electrocatalysis (see Section 8.1.1.4.2).

In this context, one quantity of particular interest is the so-called "potential of zero charge" (pzc), i.e. the electrode potential at which the electrode has no excess charge, $\sigma^m = 0$ [42]. For vanishing outer voltage ψ, the potential drop across the metal/solution interface, $\Delta\phi$, is determined by the surface potentials at the metal/solution interface. These are modified by metal–solvent interaction compared with the respective metal/vacuum (χ^{m}) and solvent/vacuum (χ^{s}) values by $\delta\chi^{m}$ and $\delta\chi^{s}$, respectively. Hence

$$\Delta\phi = (\chi^{m} - \chi^{s}) + (\delta\chi^{m} - \delta\chi^{s}) \tag{12}$$

and together with Eq. (10) the pzc can be expressed as

$$E_{\sigma=0} = \chi^{m} + \frac{\mu_{e}}{e} + \delta\chi^{m} - \delta\chi^{s} + \text{constant} \tag{13a}$$

where "constant" comprises terms from the reference electrode. Using Eqs. (4) and (5), we see that the pzc scales with the electrode work function:

$$E_{\sigma=0} = \frac{\Phi^{m}}{e} + \delta\chi^{m} - \delta\chi^{s} \tag{13b}$$

The latter expression also allows the electrode potential of the SHE to be calculated versus vacuum as reference potential [43]. The mean value found in the literature is $E_{\mathrm{abs}}^{\mathrm{SHE}} = 4.6$ V [43]. Although the calculation of the absolute potential is based on a number of assumptions, it is a useful reference point for comparing phenomena occurring at solid/gas and solid/electrolyte interfaces.

8.1.1.2.3 **Potentials in Galvanic or Electrolytic Cells** Consider an electrochemical cell in which at the anode and the cathode different electrochemical reactions are in equilibrium and the two electrode compartments are separated by an (ion conducting) membrane. This could be, for example, a "hydrogen–oxygen cell" with $H_2 \rightleftharpoons 2H^+ + 2e$ occurring at the anode and $O_2 + 4H^+ + 4e^- \rightleftharpoons 2H_2O$ at the cathode. The equilibrium potential of the cell, ΔE_{eq}, then corresponds to the difference in electronic energies between the two electrodes and a Faradaic current will flow spontaneously when the two terminals are connected through a resistor. The driving force for the current flow is the Gibbs energy of the overall cell reaction, which is, e.g. in the case of an H_2/O_2 fuel cell $H_2 + 0.5O_2 \rightleftharpoons H_2O$:

$$\Delta E_{\mathrm{eq}} = -nF\Delta G \tag{14}$$

Suppose that the right electrode, let us call it A, has a more negative potential with respect to the left electrode, which we shall call B. Then the electrons will flow through the external connection from A to B (Fig. 4a). A cell with spontaneous current flow is called a galvanic cell, important examples of which are batteries and fuel cells. If, on the other hand, an external voltage greater than ΔE is imposed between the two electrodes, electrons will flow in the opposite direction and chemical reactions are enforced at the electrodes. In this case, the cells are called electrolytic cells (Fig. 4b). They are employed, e.g., in electrolytic synthesis, electrorefining and electroplating.

To drive a Faradaic reaction at a given rate, the driving force for the reaction must be somewhat larger than the equilibrium potential. In the galvanic cell, at electrode A electrons are transferred from the solution to the electrode. To make this transfer faster, the electronic energies in A must be lowered, i.e. the electrode potential, E, becomes more positive [44]. In the electrolytic cells, it is exactly the opposite: electrons flow from electrode A into the electrolyte and thus the driving force increases as A becomes more negative. The difference between the equilibrium potential and the electrode potential necessary to drive a certain current is called the overpotential η:

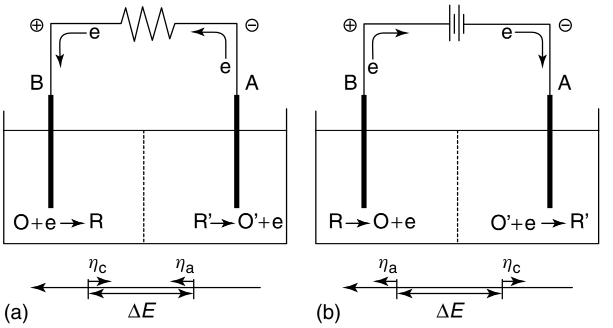

Fig. 4 (a) Galvanic cell and (b) electrolytic cell. η_a: anodic overpotential. η_c: cathodic overpotential.

$$\eta = E - E^{\mathrm{eq}} \tag{15}$$

Corresponding considerations for electrode B show that current increases as the electrode potential is lowered in the galvanic cell or raised in the electrolytic cell. Hence the overpotential decreases the cell voltage in a galvanic cell and increases it in an electrolytic cell. As a consequence, the total cell voltage decreases with increasing current in galvanic cells and increases in electrolytic cells (The sums run over anodic and cathodic overpotentials; cf. Fig. 4):

$$V_{\mathrm{galv}} = \Delta E_{\mathrm{eq}} - \sum |\eta|$$
$$V_{\mathrm{elec}} = \Delta E_{\mathrm{eq}} + \sum |\eta| \tag{16}$$

Galvanic cells are power sources. Evidently, the generated power VI is maximized when the overpotential at which a given current can be drawn is minimized. Similarly, electrolytic cells consume electrical power, the power consumption being the lesser the smaller the overpotential is. As discussed below, the overpotential might ensue from two sources: activation energies of the electrode reactions (which may originate from the sluggish charge transfer, coupled chemical reactions, etc.) and concentration profiles at the electrode owing to mass transport limitations. Hence it is distinguished between activation, η_{ct}, and concentration overpotential, η_{conc}. Further, there is a third origin of loss of cell voltage, an ohmic loss, IR, occurring in the cell or the outer electrical connections. Thus, the voltage measured between the two terminals of a galvanic cell or applied to an electrolytic cell can be divided into four contributions:

$$V = \Delta E_{\text{eq}} \pm \sum |\eta_{\text{ct}}| \pm \sum |\eta_{\text{conc}}| \pm IR \tag{17}$$

where the upper sign in ± refers to electrolytic and the lower sign to galvanic cells.

It is the goal of electrocatalysis to find electrode materials at which η_{ct} is minimum, while minimization of concentration overpotentials and ohmic losses is a question of optimizing the cell design and the mass transport conditions, i.e. an engineering problem.

8.1.1.3 Electrode Kinetics

The precondition for any approach to electrocatalysis is a theory of reaction kinetics that allows a relationship to be established between current and overpotential. Up to now the analysis of the interfacial charge transfer kinetics has been heavily based on phenomenological, macroscopic approaches. Microscopic approaches to outer-sphere charge transfer processes [45] have been developed by Marcus, largely on the basis of a classical treatment of the solvent [46], and by Hush [47]. Quantum chemical treatments of the electrode kinetics started with the work of Levich, Dogonadze, Chizmadzhev and Kuznetsov (see references in Refs. [29, 48–52]). Substantial progress has been made in developing microscopic concepts of the inner sphere reorganization contribution, and also of bond breaking and adsorption (see Ref. [53] and references therein). Yet we are still far from a fair microscopic understanding of electrocatalytic reactions. A recent boost in quantum chemical calculations gives hope for more rigorous treatments of the interfacial reaction kinetics of complex processes in the near future. In this chapter, however, we will restrict ourselves to the phenomenological theories of charge transfer. They are based on the theory of the activated complex, as known from chemical kinetics, and most easily explained with one-step electron transfer reactions, which are discussed in the next section. Section 8.1.1.3.2 deals with multistep reactions.

8.1.1.3.1 Kinetics of One-Step Electrode Reactions

Let us consider the following one step–one electron reaction:

$$\text{O} + \text{e} \underset{k_{\text{b}}}{\overset{k_{\text{f}}}{\rightleftharpoons}} \text{R} \tag{18}$$

where O and R denote the oxidized and the reduced form of a species and k_{f} and k_{b} are the heterogeneous rate constants of the forward and backward reaction, respectively, measured in cm s^{-1}. The forward reaction is associated with the flow of electrons from the electrode to a species in solution, which is called a cathodic current, I_{c}. Correspondingly, an anodic current, I_{a}, signifies that electrons flow from a species in solution to the electrode. Adopting the widespread convention that the overall current I is positive when $I_{\text{a}} > I_{\text{c}}$ and negative when the cathodic current dominates, I is given by the difference between the anodic and the cathodic current:

$$I = I_{\text{a}} - I_{\text{c}} \tag{19}$$

Anodic and cathodic currents are proportional to the reaction rates of the forward and backward reaction, v_{f} and v_{b}, which in turn can be expressed through the heterogeneous rate constants and the surface concentration of the reacting species, c_{O}^{s} and c_{R}^{s}:

$$v_{\text{f}} = \frac{I_{\text{c}}}{FA} = k_{\text{f}} c_{\text{O}}^{\text{s}} \tag{20a}$$

$$v_{\text{b}} = \frac{I_{\text{a}}}{FA} = k_{\text{b}} c_{\text{R}}^{\text{s}} \tag{20b}$$

According to the theory of the activated complex, a rate constant, k, depends exponentially on the standard free energy of activation, $\Delta G^{\#}$ [54]:

$$k = k' \mathrm{e}^{-\Delta G^{\#}/RT} \tag{21}$$

In an electrochemical reaction, $\Delta G^{\#}$ depends on the electrode potential E. The way in which E affects $\Delta G^{\#}$ can be seen most easily with standard free energy profiles along the reaction coordinate as shown in Fig. 5. The solid curve represents equilibrium conditions, where we have assumed that conditions are such that the electrode potential E attains the formal potential $E^{0'}$. The corresponding activation barriers for the forward

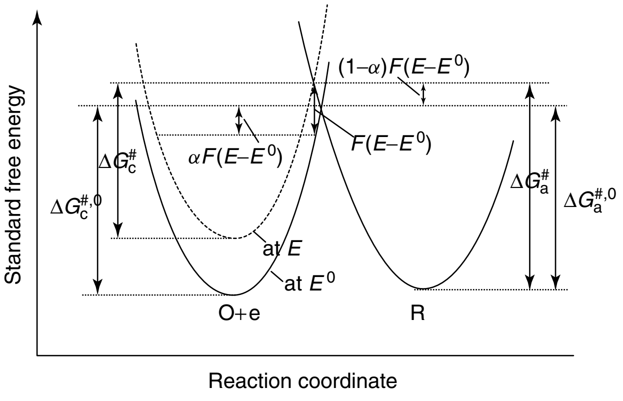

Fig. 5 Standard free energy profiles at two different potentials illustrating the effect of a potential change on the activation energy for reduction and oxidation.

References see page 1902

(cathodic) and backward (anodic) reactions are $\Delta G_{\mathrm{c}}^{\#,0}$ and $\Delta G_{\mathrm{a}}^{\#,0}$. A decrease in E increases the energy of the electron residing in the electrode by $-F(E - E^{0'})$. If the free energy profile does not change with the electrode potential and only shifts vertically by $|F(E - E^{0'})|$, then, as is evident from Fig. 5 (dashed line), the activation barrier for the reduction reaction is lowered by a fraction of the total energy change as E becomes more negative. Denoting this fraction by α, $\Delta G_{\mathrm{c}}^{\#}$ thus becomes

$$\Delta G_{\mathrm{c}}^{\#} = \Delta G_{\mathrm{c}}^{\#,0} + \alpha F(E - E^{0'}) \tag{22a}$$

Correspondingly, the activation barrier for the oxidation reaction is increased by $(1 - \alpha)$:

$$\Delta G_{\mathrm{a}}^{\#} = \Delta G_{\mathrm{a}}^{\#,0} - (1 - \alpha)F(E - E^{0'}) \tag{22b}$$

Equations (22a) and (22b) can be seen as an extension of the Brønsted–Evans–Polanyi relation to electrochemistry; α is called the transfer coefficient and is also known as the symmetry factor, since at the same time it reflects the ratio of the slopes of the two free energy curves at their intersection [40].

Inserting Eqs. (21) and (22) into Eq. (20) and introducing the standard rate constant k^0, which is the rate constant for the forward and the backward reaction in the case of equal bulk concentrations of oxidized and reduced species, $c_{\mathrm{O}}^{\mathrm{b}} = c_{\mathrm{R}}^{\mathrm{b}}$, (thus $k_f = k_b$) yields for the anodic and cathodic current densities

$$i_{\mathrm{a}} = \frac{I_{\mathrm{a}}}{A} = c_{\mathrm{R}}^{\mathrm{s}} F k^0 \mathrm{e}^{(1-\alpha)F(E-E^{0'})/RT} \tag{23a}$$

$$i_{\mathrm{c}} = \frac{I_{\mathrm{c}}}{A} = F c_{\mathrm{O}}^{\mathrm{s}} k^0 \mathrm{e}^{-\alpha F(E-E^{0'})/RT} \tag{23b}$$

At equilibrium, the partial anodic and cathodic current densities are of equal magnitude and denoted the exchange current density, i_0:

$$i_{\mathrm{a}}^{\mathrm{eq}} = i_{\mathrm{c}}^{\mathrm{eq}} = i_0 \tag{24}$$

Taking into account that under equilibrium conditions surface and bulk concentrations are equal, we obtain for the exchange current density

$$i_0 = F k^0 c_{\mathrm{O}}^{\mathrm{b}(1-\alpha)} c_{\mathrm{R}}^{\mathrm{b}\alpha} \tag{25a}$$

where, the superscript b denotes that the concentrations are bulk concentrations. Note that in the electrochemical literature, the exchange current density is often given by the following simpler expression:

$$i_0 = F k^0 c^{\mathrm{b}} \tag{25b}$$

which holds if $c_{\mathrm{O}}^{\mathrm{b}} = c_{\mathrm{R}}^{\mathrm{b}}$.

Combining Eqs. (19) and (23) results in a functional dependence of the current on the deviation of the potential from the formal electrode potential $(E - E^{0'})$. However, the interesting reference potential is the equilibrium potential and the desired relation a dependence between the current density and the overpotential, $\eta = E - E^{\mathrm{eq}}$. Moreover, so far we have taken into consideration that the surface concentrations will in general deviate from the bulk concentrations. This is the case whenever the mass transport to or from the electrode affects the reaction rate. When studying the kinetics of a reaction, one wishes to eliminate mass transport effects. When assuming rapid mass transport and substituting E by η, we obtain the well-known and for electrochemical kinetics most important Butler–Volmer equation [55]:

$$i = i_0 \left[\mathrm{e}^{(1-\alpha)F\eta/RT} - \mathrm{e}^{-\alpha F\eta/RT}\right] \tag{26}$$

The Butler–Volmer equation gives us an important insight into several aspects of electrode kinetics:

First, and most important in the context of electrocatalysis, it tells us that there are two quantities that determine the "catalytic rank" of an electrode material, namely the exchange current density, i_0, and the transfer coefficient, α. Clearly, the larger i_0 for a given α, the lower is the overpotential necessary to maintain a certain current density and thus the better is the catalyst. i_0 is proportional to k^0; it is therefore a direct measure of the standard rate constant of an electrode reaction. However, misjudgments might arise when the quality of an electrocatalyst is rated by i_0 alone. Different values of α can lead to a crossing of the i/η curves measured for the same reaction and different electrode materials with different i_0s (Fig. 6). Therefore, depending on the desired current density, different electrode materials should be chosen. Hence the quality of electrocatalysts with different values of α can only be ranked when the desired operating conditions are known.

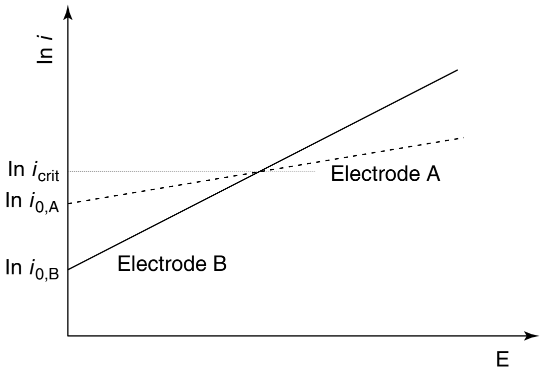

Fig. 6 Tafel plots of two electrodes with different exchange current densities and different transfer coefficients. If the desired current density $i_{\mathrm{set}} < i_{\mathrm{crit}}$, electrode A is the better catalyst and for $i_{\mathrm{set}} > i_{\mathrm{crit}}$ electrode B is more suitable.

Second, for small values of η, the exponential can be expanded in a Taylor series up to the linear term, which yields a linear dependence of current on overpotential:

$$i = \frac{i_0 F}{RT}\eta \tag{27}$$

The resulting equation has the same form as Ohm's law, which led to the definition of the charge transfer resistance R_{ct}:

$$R_{\text{ct}} = \frac{RT}{i_0 F} \tag{28}$$

Hence i_0 can be in principle accessed from the slope of a measured $i-\eta$ curve in the range $|\eta| \leq 5$ mV, provided that the reaction proceeds in a single step.

Third, for large values of η, i.e., $|\eta| \geq 50$ mV, one of the terms in brackets can be neglected and an exponential current–potential characteristic is obtained, yielding for large negative η

$$i = i_0\,\mathrm{e}^{-\alpha F\eta/RT} \tag{29a}$$

and for large positive η

$$i = i_0\,\mathrm{e}^{(1-\alpha)F\eta/RT} \tag{29b}$$

Thus, a plot of log i vs. η, known as a Tafel plot, yields a straight line:

$$\eta = a + b\log i \tag{30}$$

Evaluation of the slope b allows the determination of α and interpolation of the linear segments to the equilibrium potential, i.e. $\eta = 0$, yields i_0. Tafel plots are a very useful diagnostic tool to determine kinetic parameters. They are also helpful for reactions that do not proceed in a single step; then, however, the interpretation of the slope and the intercept changes – see Section 8.1.1.3.2.

On increasing the overpotential in the positive or negative direction, a corresponding exponential increase in current density as predicted by the Butler–Volmer equation can only take place as long as the transport of educts to and products from the electrode is sufficiently fast such that the surface concentrations are identical to the bulk concentrations. It is obvious that sooner or later in any system the mass transport rate will come in the range of the particle fluxes owing to the electrochemical reaction when increasing $|\eta|$. Then, we have a mixed control of mass transport and electrode kinetics. At very large $|\eta|$, finally, the current is totally determined by the mass transfer rate and a limiting current independent of η adjusts. It can be shown that when mass transport becomes important the $\mathrm{i} - \eta$ relation obeys

$$i = i_0\left[\left(1 - \frac{i}{i_{\text{l,a}}}\right)\mathrm{e}^{(1-\alpha)F\eta/RT} - \left(1 - \frac{i}{i_{\text{l,c}}}\right)\mathrm{e}^{-\alpha F\eta/RT}\right] \tag{31}$$

where $i_{\text{l,a}}$ and $i_{\text{l,c}}$ are the anodic and cathodic limiting current densities [40].

Again, Eq. (31) can be linearized for small η, which leads to

$$\eta = \frac{RT}{F}\left(\frac{1}{i_0} - \frac{1}{i_{\text{l,c}}} + \frac{1}{i_{\text{l,a}}}\right)i \tag{32}$$

Corresponding to the definition of the charge transfer resistance above, we can define an anodic and cathodic mass transfer resistance and rewrite Eq. (32) as follows:

$$\eta = i(R_{\text{ct}} + R_{\text{mt,a}} + R_{\text{mt,c}}) \tag{33}$$

Clearly, if $R_{\text{ct}} \ll R_{\text{mt,a(c)}}$, that is, $i_0 \gg i_{\text{l,a(c)}}$, then the current is dominated by the mass transfer resistance and the corresponding overpotential is determined by the difference between the surface and the bulk concentrations and termed concentration overpotential η_{conc}. In the opposite case, i.e. when $R_{\text{ct}} \gg R_{\text{mt}}$, the overpotential is dominated by the activation of charge transfer and is referred to as activation or charge transfer overpotential η_{ct} [see also Eq. (17)].

For large overpotentials, one of the two terms in brackets in Eq. (31) can again be neglected and plots of $\log[(i_{\text{l,c}} - i)/i]$ (which is usually referred to as mass transport-corrected current) vs. η yield straight lines. From their slopes and intercepts the kinetic parameters α and i_0 can be evaluated even in the presence of mass transfer.

8.1.1.3.2 Multistep Reactions

So far, we have considered reactions that involve just one electron that is transferred in the overall reaction and assumed that the mechanism constitutes of only a single step. Many electrochemical reactions require the transfer of more than one electron for the overall reaction to occur once. In addition, the reaction mechanism often contains also purely chemical steps. Thus, a general electrochemical reaction in which n electrons are transferred will proceed in at least n electrochemical steps, which might be coupled to m chemical steps. The succession of electrochemical and chemical elementary steps determines the reaction mechanism. Especially electrocatalytic reactions that involve the adsorption of an intermediate at the electrode surface are multistep reactions. A general theory of current–potential relations for multistep reactions would need to take into account all potential dependences and surface concentrations of the intermediates in addition to the bulk concentrations of educts and products, many of which will not be experimentally available. Fortunately, in most experimental situations the problem can be significantly simplified because one of the steps is much more sluggish than all the others. The current is then determined by the rate of this slowest step, which we shall abbreviate as RDS (rate-determining step). As a rule of thumb, a step qualifies as RDS if it is at least 10 times slower than all the other reactions.

In the following we assume that an RDS exists. Let us consider the overall reaction

$$\mathrm{O} + n\mathrm{e} \rightleftharpoons \mathrm{R} \tag{34}$$

A general mechanism will contain n' electron transfer reactions preceding the RDS, possibly intermixed with m' chemical steps, one RDS that might be of electrochemical or chemical nature and n'' (with $0 \leq n' \leq n - n''$) charge transfer steps in addition to m'' chemical steps following the RDS. It is thus of the general character

$$\begin{aligned}
&\mathrm{O} + n'\mathrm{e} \rightleftharpoons \mathrm{O}' \\
&\mathrm{O}' + r\mathrm{e} \underset{k_b^{\mathrm{RDS}}}{\overset{k_f^{\mathrm{RDS}}}{\rightleftharpoons}} \mathrm{R}' \\
&\mathrm{R}' + n''\mathrm{e} \rightleftharpoons R
\end{aligned} \tag{35}$$

where $r = 0$ if the RDS is of chemical nature and 1 if it is a charge transfer step. Obviously, $n = n' + n'' + r$. The existence of an RDS indicates that all the other steps are virtually at equilibrium. In the case of an electrochemical RDS, its current density is thus given by

$$\begin{aligned}
i_{\mathrm{RDS}} = {} & \mathrm{constant}_{\mathrm{f}} \times c^{\mathrm{s}}_{\mathrm{O}'} \mathrm{e}^{-\alpha F\eta/RT} - \mathrm{constant}_{\mathrm{b}} \\
& \times c^{\mathrm{s}}_{\mathrm{R}'} \mathrm{e}^{(1-\alpha)F\eta/RT}
\end{aligned} \tag{36}$$

where α is the transfer coefficient of the RDS and the constants depend on the respective rate constants k^{RDS}, the Faraday constant and the standard electrode potential of the RDS. At a steady state, all sequential electron transfer steps proceed at the same rate and therefore the total current is given by

$$i = n i_{\mathrm{RDS}} \tag{37}$$

Since steps preceding and following the RDS are at equilibrium, the surface concentrations $c^{\mathrm{s}}_{\mathrm{O}'}$ and $c^{\mathrm{s}}_{\mathrm{R}'}$ can be expressed in terms of the bulk concentration $c^{\mathrm{b}}_{\mathrm{O}'}$ and $c^{\mathrm{b}}_{\mathrm{R}'}$, respectively, and the equilibrium constants of the individual reactions [56]. On inserting the corresponding expressions into Eq. (36), combining it with Eq. (37) and rearranging terms, one arrives at a Butler–Volmer-type current–potential relation:

$$i = i_0\left(\mathrm{e}^{\overleftarrow{\gamma} F\eta/RT} - \mathrm{e}^{-\overrightarrow{\gamma} F\eta/RT}\right) \tag{38}$$

The so-called observable charge transfer coefficients $\overrightarrow{\gamma}$ and $\overleftarrow{\gamma}$ of the forward and backward reactions, respectively, now depend, however, on the specific reaction mechanism. This makes generalized Tafel plots a useful tool for the validation of postulated reaction mechanism of multistep reactions in general and of electrocatalytic reactions in particular. Note that also the exchange current density i_0 in Eq. (38) is not given by Eq. (25) any longer, but depends on the equilibrium constants of the steps in equilibrium, the bulk concentrations $c^{\mathrm{b}}_{\mathrm{O}'}$ or $c^{\mathrm{b}}_{\mathrm{R}'}$, the rate constants of the RDS and its transfer coefficient and the number of electrons transferred in the steps preceding the RDS, n'.

The above derivation of Eq. (38) leads also to explicit expressions for the observable transfer coefficients [56]:

$$\overrightarrow{\gamma} = \frac{n'}{\nu} + r\alpha \quad \text{and} \quad \overleftarrow{\gamma} = \frac{n - n'}{\nu} - r\alpha \tag{39}$$

where

$$\overrightarrow{\gamma} + \overleftarrow{\gamma} = \frac{n}{\nu} \tag{40}$$

and ν is the stoichiometric number of the RDS. This determines how many times the RDS takes place for the overall reaction to occur once. To elucidate this definition, consider the overall reaction

$$2\mathrm{A}^+ + 2\mathrm{e} \rightleftharpoons \mathrm{A}_2 \tag{41}$$

Let us assume that it takes place in two consecutive steps, the first of which is the RDS:

$$\begin{aligned}
\mathrm{A}^+ + \mathrm{e} &\rightleftharpoons \mathrm{A}_{\mathrm{ad}} \\
2\mathrm{A}_{\mathrm{ad}} &\rightleftharpoons \mathrm{A}_2
\end{aligned} \tag{42}$$

Then, clearly, the first step must take place twice for the overall reaction to occur once. Hence $\nu = 2$.

The diagnostic value of Tafel plots for the determination of the reaction mechanism of a multistep electron transfer reaction can now be appreciated. For any postulated reaction mechanism, the values of the observable charge transfer coefficients can be calculated (provided that α is known) and they can be extracted from the experimental data by analyzing the slopes of the linear portions of $\log i$ vs. η curves. Hence considerable experimental evidence for or against a certain reaction mechanism and in particular the RDS can be obtained. The determination of the latter, in turn, is among the most important tasks in electrocatalytic research, since any attempt to accelerate an electrocatalytic reaction is tantamount to making the RDS faster.

The above discussion should not give the impression that the reaction mechanism can always be obtained in the above-mentioned way. Often there are experimental constraints that make such a complete analysis impossible. For example, it might not be possible to eliminate the mass transport limitation (note that so far we have assumed that the current is entirely charge transfer controlled), forward and backward reactions can follow different mechanisms in the Tafel regimes, the slowest reaction might not be sufficiently separated in rate such that equilibrium conditions cannot be assumed for the remaining reactions, etc. Also, the same Tafel slopes may occur for different RDS (see Section 8.1.1.5.1). These aspects render multistep electron transfer kinetics a complicated topic. How one can deal with more complicated situations, in which the above analysis cannot be applied, is discussed in Ref. [40], where references to more specific elaborations are also given.

8.1.1.4 Fundamentals of Electrocatalysis

Electrocatalysis is characterized by the fact that widely different reaction rates are observed for different electrodes at the same electrode potential (i.e. equal electron energies) and also otherwise identical parameters (concentration, temperature, etc.). The primary origin of electrocatalysis is the adsorption of educts, intermediates or products on the electrode, the heats of adsorption depending on the chemical nature or the structure of the electrode. The signature of electrocatalysis is a “volcano-shaped” dependence of the reaction rate (or current) on the adsorption energy of key reaction intermediates, a so-called volcano curve. The rationalization of volcano curves in catalysis was first given by Sabatier in the early 1900s. The Sabatier principle states that an active catalyst should adsorb a key intermediate neither too weakly nor too strongly. Studies in heterogeneous catalysis and electrocatalysis demonstrated innumerous examples of volcano curves. In Section 8.1.1.4.1 we will discuss the origin of volcano curves from an electrochemical perspective. In addition to the bonding strength of intermediates, the structure of the double layer, which varies at identical electrode potential for different materials, affects the overall reaction rate. These effects are referred to as “secondary effects” and are reviewed in Section 8.1.1.4.2.

8.1.1.4.1 Primary Effects: Heat of Adsorption and Volcano Plots

The qualitative dependence of electrocatalytic activity on the adsorption energy, which, independent of the reaction considered, follows a volcano curve, can be rationalized most easily when analyzing a simple example. Consider a one-electron reduction of a species O to R that proceeds through an intermediate Y:

$$\mathrm{O} + \mathrm{e} \underset{k_{-1}}{\overset{k_1}{\rightleftharpoons}} \mathrm{Y} \xrightarrow{k_2} \mathrm{R} \tag{43}$$

If Y adsorbs at the electrode, its standard Gibbs energy of formation and hence also the activation energy of the formation will be lowered. Evidently, as long as the formation of Y is the rate-determining step, the overall reaction rate increases as the adsorption energy increases since the adsorbed intermediate is stabilized by the electrode surface. However, the bond strength of Y to the electrode necessarily affects also the rate with which R is formed from Y: the latter reaction becomes slower as the bond strength becomes stronger. These contrary responses of formation and removal of Y with increasing heat of adsorption lead to an increase in the coverage of Y with increasing heat of adsorption. A high coverage, in turn, slows down the rate of formation of Y, which is proportional to the free surface sites, but increases the reaction rate of formation of R. These simple considerations already indicate that the production rate of R, and thus the electrocatalytic activity of the electrode, will be maximum at an intermediate value of the heat of adsorption. For the reaction scheme above, a quantitative relationship can be easily deduced, giving further insight into how the three partial reaction rates are affected by a change in the adsorption energy and how their interaction yields a volcano curve.

Let us first consider the steady-state coverage that will establish for different ratios of the three rate constants. The rates of formation of Y and its removal due to oxidative desorption or consecutive reaction are given by

$$\begin{aligned} \nu_{\mathrm{ad}} &= c_{\mathrm{O}} k_1 (1-\theta) \\ \nu_{\mathrm{des}} &= k_{-1}\theta \\ \text{and}\qquad \nu_{\mathrm{reac}} &= k_2\theta \end{aligned} \tag{44}$$

respectively, where θ is the fraction of surface sites which are covered by Y and c_{O}, as before, the concentration of educt in the reaction plane. At the steady state

$$\frac{\mathrm{d}\theta}{\mathrm{d}t} = \nu_{\mathrm{ad}} - \nu_{\mathrm{des}} - \nu_{\mathrm{reac}} = 0 \tag{45}$$

which yields

$$\theta_{\mathrm{ss}} = \frac{1}{1 + \dfrac{k_{-1}}{k_1 c_{\mathrm{O}}} + \dfrac{k_2}{k_1 c_{\mathrm{O}}}} \tag{46}$$

Equation (46) tells us that as long as the formation of Y remains much slower than both its reductive

---

References see page 1902

desorption and consecutive reaction to R, i.e. as long as $k_1c_O \ll k_{-1} + k_2$, the coverage remains negligible. In the opposite limit, i.e. if the adsorption is much faster than either desorption or reaction, i.e. $k_1c_O \gg k_{-1} + k_2$, the electrode surface is nearly fully covered with Y. As the adsorption strength increases, k_1 increases and both k_2 and k_{-1} decrease. Hence θ increases monotonically with increasing adsorption strength.

To obtain a quantitative relation between the electrocatalytic activity, which depends on θ_{ss} and the adsorption strength, we have to express the rate constants k_i in terms of the Gibbs free energy of adsorption of Y, ΔG_{ad}, i.e. the change in the standard Gibbs energy due to the adsorption of Y on the electrode surface. Figure 7 illustrates how the activation energies of the three partial reactions depend on ΔG_{ad}. The dashed curve indicates the energetic situation if Y has no interaction with the surface. In this case the Gibbs activation energy is denoted by $\Delta G_1^{\#}$. According to the Brønsted–Evans–Polanyi rule, there is a linear relationship between the activation energy and the change in the free energy for an elementary reaction, i.e.

$$\Delta G^{\#}_{1,\mathrm{ad}} = \Delta G^{\#}_1 + \alpha\Delta G_{\mathrm{ad}} \tag{47}$$

Equally, the activation energies of desorption and reaction can be written as

$$\Delta G^{\#}_{-1,\mathrm{ad}} = \Delta G^{\#}_1 - (1-\alpha)\Delta G_{\mathrm{ad}} \tag{48}$$

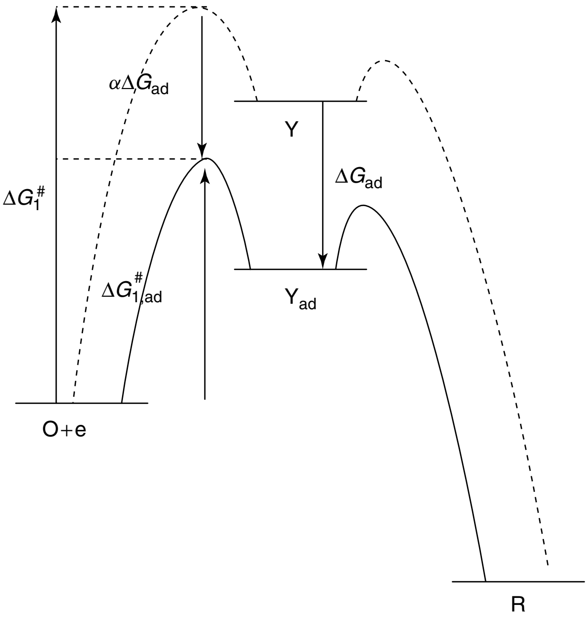

Fig. 7 Standard Gibbs energies for reaction scheme (44) for the case that the intermediate Y does not adsorb at the electrode (dashed curves) and for the case that Y adsorbs at the electrode (solid curves).

and

$$\Delta G^{\#}_{2,\mathrm{ad}} = \Delta G^{\#}_2 - (1-\beta)\Delta G_{\mathrm{ad}} \tag{49}$$

The change in the activation energy upon adsorption is also illustrated in Fig. 7. Equations (49) and (50) allow us to choose the rate constants for the case when Y does not interact with the surface, k'_i, as convenient reference constants:

$$\begin{aligned} k_1 &= A_1 \mathrm{e}^{-\Delta G^{\#}_{1,\mathrm{ad}}/RT} = A_1 \mathrm{e}^{-\Delta G^{\#}_1/RT} \mathrm{e}^{-\alpha\Delta G_{\mathrm{ad}}/RT} \\ &= k'_1 \mathrm{e}^{-\alpha\Delta G_{\mathrm{ad}}/RT} \end{aligned} \tag{50}$$

$$k_{-1} = k'_{-1}\mathrm{e}^{(1-\alpha)\Delta G_{\mathrm{ad}}/RT} \tag{51}$$

$$k_2 = k'_2\mathrm{e}^{(1-\beta)\Delta G_{\mathrm{ad}}/RT} \tag{52}$$

Note that $\Delta G_{ad} < 0$ and thus k_1 increases and k_{-1} and k_2 decrease with increasing adsorption strength, as required. To a first approximation, we can assume that $\alpha = \beta = 0.5$. Inserting Eqs. (50)–(52) into Eq. (46) θ_{ss} can be calculated as a function of ΔG_{ad}:

$$\theta_{ss} = \frac{1}{1 + \left(\dfrac{k'_{-1}}{k'_1 c_O} + \dfrac{k'_2}{k'_1 c_O}\right)\mathrm{e}^{\Delta G_{\mathrm{ad}}/RT}} \tag{53}$$

The stationary current density follows directly from the rate laws Eq. (44):

$$\begin{aligned} i = i_{\mathrm{ox}} - i_{\mathrm{red}} = F \Big\{ & k'_1 \mathrm{e}^{\alpha\Delta G_{\mathrm{ad}}/RT}[1 - \theta_{\mathrm{ss}}(\Delta G_{\mathrm{ad}})] \\ & - k'_{-1}\mathrm{e}^{-\alpha\Delta G_{\mathrm{ad}}/RT}\theta_{\mathrm{ss}}(\Delta G_{\mathrm{ad}}) \Big\} \end{aligned} \tag{54}$$

Plots of $\ln i$ and of θ_{ss} vs. ΔG_{ad} as calculated from Eqs. (53) and (54) are shown in Fig. 8. As expected,

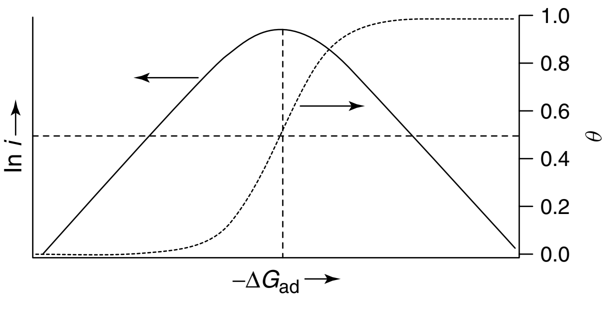

Fig. 8 Catalytic activity (solid curve) and coverage of intermediate Y (dashed curve) as a function of the standard Gibbs energy of adsorption of Y for reaction scheme (44). The curves were calculated with Eqs. (54) and (53) for $k'_{-1}/k'_1c_O + k'_2/k'_1c_O = 10\,000$, i.e. a situation in which without adsorption the formation of Y is the rate-limiting step. (Note that shapes and relative positions of the curves do not depend on the quantitative values of the rate constants as long as without adsorption the formation of Y is rate determining.)

the catalytic activity goes through a maximum with increasing adsorption strength whereas the coverage increases monotonically with $|\Delta G_{\mathrm{ad}}|$ and exhibits a sigmoidal shape.

Equations (53) and (54) imply that as long as θ_{ss} is low, adsorption is rate determining whereas a high θ_{ss} is found only if the reaction is rate determining. Hence the RDS necessarily changes with increasing adsorption energy, i.e. as we go through the maximum of the volcano curve. In this view, discussions of volcano curves that assume the same RDS over the entire range of ΔG_{ad}, as found fairly often in the electrochemical literature (e.g. in Chapter 10 in Ref. [1]) have to be treated with caution.

At maximum current, $\theta_{\mathrm{ss}} = 0.5$ and thus

$$k_1 c_{\mathrm{O}} - k_{-1} = k_2 \tag{55}$$

Note that for more complex mechanisms with more than one type of adsorbate, optimum coverage of key reaction intermediates may differ significantly from 0.5.

Hence the best catalyst is the one for which the rate constants of "net adsorption" (i.e. the difference in the adsorption rate at zero coverage and the rate constant of desorption) is equal to the rate constant of the reaction. This suggests that the standard Gibbs free energies of formation of Y from O and formation of R from Y should be similar.

So far, our discussion has neglected the influence of the electrode potential on the reaction rate. This dependence is implicitly included in the rate constants k'_1 or k'_{-1} that can be written as

$$k'_1 = k_1^{0'} \mathrm{e}^{-\alpha F(E-E^{0'})/RT}$$

$$\text{and} \qquad k'_{-1} = k_{-1}^{0'} \mathrm{e}^{(1-\alpha)F(E-E^{0'})/RT} \tag{56}$$

respectively. Hence the catalytic activity of different electrode materials should always be compared at *equal electrode potentials.* Owing to the different chemical potentials of electrons in different materials, the magnitude of surface charge and possibly even the sign of the surface charge will differ at equal E for different electrocatalysts. As a consequence, the double layer structure also differs, which in turn affects the reaction rate. Changes of the reaction rate that originate from a changed double-layer structure are called secondary effects and are discussed in the next section. One consequence of the different double-layer structures for different materials that is usually not considered when secondary effects are discussed is that the adsorption strength of an adsorbate is influenced by the surface charge, a fact that further complicates an analysis of catalyzed electrode reactions. Experimental evidence thereof is the Stark tuning effect observed in IR spectra, that is, variation of vibrational frequencies of adsorbates with the electrode potential [57].

Differences in catalytic activity of the same material in an electrochemical environment and in heterogeneous catalysis are therefore not only due to the fact that the educts and products are solved in an electrolyte, but also arise because of different surface charge densities. In electrocatalysis, the surface charge at the metal/electrolyte interface is to a large extent controlled by the electrode potential under the operating conditions and influenced by the adsorbed ions/molecules. In heterogeneous catalysis, the surface charge is entirely determined by the nature of the adsorbates. The connection between solid/liquid electrified and solid/gas interfaces has been discussed in relation to the so-called double layer modeling in ultra-high vacuum, which was pioneered by Sass and coworkers in the 1980s [58, 59].

8.1.1.4.2 **Secondary Effects: Double Layer Structure**

At equal driving force for the reaction, different electrode materials develop different potential drops across the double layer (see also Section 8.1.1.2.2) and, furthermore, they exhibit a different tendency to chemisorb ions, which again, as discussed above, influences the double-layer structure. An influence of the electrode material on the reaction rate may therefore even be observed in the absence of any interaction of a species involved in the overall reaction with the electrode surface. Such electrocatalytic effects are called "secondary effects" or, in recognition of Frumkin's pioneering work, "Frumkin effects". Their origin lies in the different double-layer structures that establish at electrodes of different nature. Above we derived that the current density is proportional to the concentration of the educt in the reaction plane and depends exponentially on the potential:

$$|i| \sim c\mathrm{e}^{|E-E^0|} \tag{57}$$

In interpreting Eq. (57), we assumed (a) that if c is not identical with the bulk concentration, mass transfer comes into play, and (b) that the entire potential drop across the double layer occurs between the electrode and the reaction plane. Both assumptions are idealizations which are met best in electrolytes with high ionic strength at potentials far away from the pzc and in the absence of specific adsorption at the electrode surface. If conditions (a) and (b) are not met, the following effects come into play that alter the current density:

1. For charged species and electrolytes with medium or low conductivity, Coulomb forces exerted by the surface charge of the electrode on the charged reactants cause

References see page 1902

a static concentration profile across the double layer with an increased or decreased concentration in the reaction plane with respect to the bulk concentration, depending on the signs of the charges on the electrode and the reacting ions. Let us denote the distance of closest approach from which the electron transfer occurs from the electrode surface by x_2, the potential in the reaction plane, i.e. at x_2 by ϕ_2, and let us set the potential in the bulk electrolyte to zero, $\phi_0 = 0$. Then, the concentration of the reacting species at x_2 is

$$c(x_2) = c_\mathrm{b}\mathrm{e}^{-zF\phi_2/RT} \tag{58}$$

where z is the charge on the reacting species, for anions $z < 0$, for cations $z > 0$.

2. The lower the electrolyte conductivity, the greater is the extension of the double layer into the electrolyte. Hence only the fraction $\Delta\phi - \phi_2$ of the entire potential drop across the double layer $\Delta\phi$ drops between electrode and x_2 and thus also only a fraction of the change in electric energy of an electron between electrode and electrolyte, $F\Delta\phi$, is operating in the reaction plane. In the case of a reduction reaction the current is thus proportional to

$$\begin{aligned} i &\sim \mathrm{e}^{-(E-\phi_2-E^0)\alpha F/RT} \\ &= \mathrm{e}^{-\phi_2\alpha F/RT}\mathrm{e}^{-(E-E^0)\alpha F/RT} \end{aligned} \tag{59}$$

A corresponding expression holds for oxidation currents.

Hence, compared with the ideal situation, the current density differs by a correction factor, which is called the Frumkin correction:

$$i = i_\mathrm{ideal}\,\mathrm{e}^{-(\alpha-z)F\phi_2/RT} \tag{60}$$

The Frumkin correction can be calculated if ϕ_2 is known. In the absence of specific adsorption, ϕ_2 can be determined readily from measurements of the charge density and the Gouy–Chapman–Stern theory [40]. However, a theory that would allow one to extract ϕ_2 in the presence of specific adsorption, either of ions of the supporting electrolyte or of reacting species, is not available. This makes it difficult to predict the influence of double-layer effects in electrocatalytic reactions. Whenever possible, in an electrocatalytic investigations one will avoid them by using a large excess of supporting electrolyte.

8.1.1.5 The Hydrogen Oxidation/Evolution Reaction

The hydrogen evolution reaction (HER):

$$2H_2O + 2e \longrightarrow H_2 + 2OH^- \tag{61}$$

$$2H^+ + 2e \longrightarrow H_2 \tag{62}$$

[Eq. (61) in alkaline and Eq. (62) in acidic medium] was the first electrochemical reaction ever investigated. It was mentioned in 1800 by Nicholson and Carlisle [60], who used a Volta pile to perform water electrolysis. For many years, the HER was studied as a model reaction in electrochemistry. For example, it provided a basis for establishing the famous phenomenological Tafel equation [61] relating the current to the electrode potential [see Section 8.1.1.3.1, Eq. (30)]. In 1930, Kobosev and Nekrasova first recognized the influence of the hydrogen adsorption energy on the rate of the HER [62]. It was again the HER which inspired Kobosev and Monblanova to coin the term "electrocatalysis" [63]. The HER is important for water electrolysis and it also occurs as a side-reaction for many cathodic processes (hydrogenation, etc.). The reverse reaction – the oxidation of molecular hydrogen (HOR) – has been studied less extensively due to the interference of mass transport. However, during recent decades the HOR has attracted much attention in connection with the development of hydrogen fuel cells, in particular polymer electrolyte membrane fuel cells (PEMFCs) [1].

The HER and HOR and also related processes of hydrogen adsorption have been reviewed comprehensively (see, e.g., Refs. [13, 64–72] and references therein). Below, we first discuss possible mechanisms of the HER/HOR (Section 8.1.1.5.1) and then review how the reaction rates and mechanisms are related to different electrode materials (Section 8.1.1.5.2). In the last part (Section 8.1.1.5.3), we present some details on hydrogen adsorption on electrode surfaces.

8.1.1.5.1 Reaction Kinetics and Mechanisms

The HER/HOR may occur by two different reaction sequences, the Tafel (63) – Volmer (64) or the Heyrovsky (65) – Volmer (64) reactions, which are given below for the case of an acidic electrolyte. Here $*$ and H_ad stand for free adsorption sites and hydrogen atoms adsorbed on the electrode surface, respectively.

$$H_2 + 2^* \rightleftharpoons 2H_\mathrm{ad} \tag{63}$$

$$H_\mathrm{ad} \rightleftharpoons {}^* + H^+ + e^- \tag{64}$$

$$H_2 + {}^* \rightleftharpoons H^+ + H_\mathrm{ad} + e^- \tag{65}$$

Hence the HER and the HOR are examples of complex multielectron–multistep electrochemical reactions, comprising charge transfer steps (64) and (65), chemical step (63) and also mass transport of H_2 and H^+ from and to the electrode surface. The kinetic equation for the HER/HOR and hence the dependence of the overall current on the electrode potential vary markedly depending on which reaction is the RDS. Let us discuss some typical cases, which are summarized in Table 1 (see Refs. [66] and [73] for details).

Case A in Table 1 assumes that the charge transfer reaction (64) is the RDS and the Butler–Volmer equation Eq. (26) holds. Equation (i) in Table 1 is obtained from Eq. (26) when considering the coverage of the electrode surface with hydrogen (θ_{H}) and the fact that the evolution of one $\mathrm{H_2}$ molecule involves two electrons. θ_{H}^{0} is the hydrogen coverage at equilibrium, i.e. at $\eta = 0$. Note that θ_{H} is a function of the electrode potential, which in general leads to a potential-dependent Tafel parameter. However, for metals poorly adsorbing hydrogen θ_{H} is low in a wide potential window and Tafel slopes close to 118.3 mV decade^{-1} at 298 K (corresponding to $\alpha_{\mathrm{V}} = 0.5$) are observed.

Case B corresponds to the case when the chemical reaction (63) is the RDS. This implies that the rate constant for the Tafel reaction is much smaller than that for the Volmer reaction and the latter may be considered to be in quasi-equilibrium. Under these simplifying conditions, the relation between the current and overpotential is usually expressed as

$$\eta = \frac{RT}{2F} \ln\left(1 + \frac{i}{i_{\mathrm{T}}}\right) \tag{66}$$

Note that Eq. (66) takes into consideration only the cathodic reaction. Here the rate of the heterogeneous Tafel reaction is formally converted into electric current:

$$i_{\mathrm{T}} = 2Fk_{\mathrm{T}}(\theta_{\mathrm{H}})^2 \tag{67}$$

It is often assumed that θ_{H} does not differ markedly from the equilibrium coverage θ_{H}^{0} and hence $i_{\mathrm{T}} \approx i_{0\mathrm{T}} = 2Fk_{\mathrm{T}}(\theta_{\mathrm{H}}^{0})^2$. However, when writing θ_{H} as a function of the overpotential, it is also possible to obtain an analytical solution for the current without resorting to this simplification. Assuming a Langmuir isotherm, θ_{H} is given by

$$\theta_{\mathrm{H}} = \frac{\theta_{\mathrm{H}}^{0}}{\theta_{\mathrm{H}}^{0} + (1 - \theta_{\mathrm{H}}^{0}) \exp(\eta F/RT)} \tag{68}$$

which leads to Eq. (ii) in Table 1. A more general description is obtained when using a Temkin [74] or a Frumkin [75] isotherm. According to Eqs. (66) and (ii) in Table 1, a Tafel slope of 29.6 mV decade^{-1} is expected and has indeed been observed for the platinum metals. It should be noted, however, that although Eqs. (66) and (ii) give useful guidelines for the analysis of the HER/HOR on metals that strongly adsorb hydrogen, the treatment presented is oversimplified and in fact θ_{H} established is the result of the interplay of reactions (63) and (64). Analysis of Eq. (ii) in Table 1 leads to the conclusion that at high cathodic and anodic overpotentials limiting reaction currents must be observed independent of mass transfer limitations:

$$i_{\mathrm{l,c}} = -\frac{i_{0\mathrm{T}}}{(\theta_{\mathrm{H}}^{0})^2};\ i_{\mathrm{l,a}} = \frac{i_{0\mathrm{T}}}{(1 - \theta_{\mathrm{H}}^{0})^2} \tag{69}$$

This prediction has been widely discussed in the literature (see, e.g., Refs. [73, 76]), but has not been unambiguously supported experimentally. For the HOR the limiting anodic current is determined by the mass transport rather than by the slow chemical reaction (see case E, Table 1).

For cases C and D in Table 1, i.e. when reactions (64) and (65), respectively, are rate determining in the case of the Volmer–Heyrovsky sequence, kinetic equations similar to case A are obtained. More complex situations arise when the exchange current densities for different reaction steps have comparable values [66, 68, 73].

8.1.1.5.2 Influence of the Electrode Material on the HER/HOR

The HER has been studied on various metal and alloy electrodes and the exchange current density has been shown to vary by up to 10 orders of magnitude. Many authors have attempted to establish correlations between the rate of the HER and physical and chemical properties of electrode materials. The dependence of the HER on the metal work function Φ was first discussed by Bockris in 1947 [77]. In his seminal papers, Trasatti presented critical analysis of experimental data on metal work functions and potentials of zero charge [78] and demonstrated that $\log i_0$ varies linearly with Φ, irrespective of the detailed nature of the mechanism involved in the rate-determining step [79]. Moreover, transition metals and sp metals with positively charged surfaces and sp metals with negatively charged surfaces (Fig. 9) fall on two different straight lines that are shifted in parallel along the Φ axis. The shift has been interpreted in terms of differing orientations of water dipoles at the interface of the two groups of metals.

An issue which has attracted much attention and which has been approached by a number of authors is the relationship between the catalytic activity of materials towards the HER and hydrogen adsorption energies. Conway and Bockris [80] demonstrated that the linear dependence of $\log i_0$ on Φ originated from a correlation between Φ and M–H adsorption energy. Parsons [81] showed that volcano-type curves (see Fig. 8 and Section 8.1.1.4.1) should arise when $\log i_0$ values for a series of metals are plotted against the standard Gibbs energy of hydrogen adsorption. It took quite a

References see page 1902

Tab. 1 Kinetic Equations and Tafel Parameter *b* for HER/HOR[a]

Mechanism	***Rate-determining step***	***Kinetic equation***	***Tafel parameter b***	
			Anodic reaction (HOR)	***Cathodic reaction (HER)***
Volmer–Tafel	Volmer (A)	$i = 2i_{0,\mathrm{V}}\left[\frac{\theta_\mathrm{H}}{\theta_\mathrm{H}^0}\exp\frac{(1-\alpha_\mathrm{V})\eta F}{RT} - \frac{1-\theta_\mathrm{H}}{1-\theta_\mathrm{H}^0}\exp\frac{-\alpha_\mathrm{V}\eta F}{RT}\right]$ (i)	$\frac{2.3RT}{(1-\alpha_\mathrm{V})F}$ (for $\theta_\mathrm{H} \approx$ constant)	$-\frac{2.3RT}{\alpha_\mathrm{V}F}$ (for $\theta_\mathrm{H} \approx$ constant)
Volmer–Tafel	Tafel (B)	$i = i_{0\mathrm{T}}\frac{\exp(2\eta F/RT) - 1}{[\theta_\mathrm{H}^0 + (1-\theta_\mathrm{H}^0)\exp(\eta F/RT)]^2}$ (ii)	$\frac{2.3RT}{2F}$ (for $\theta_\mathrm{H} \approx$ constant)	$-\frac{2.3RT}{2F}$ (for $\theta_\mathrm{H} \approx$ constant)
Volmer–Heyrovsky	Volmer (C)	See case A	See case A	See case A
Volmer–Heyrovsky	Heyrovsky (D)	$i = 2i_{0,\mathrm{H}}\left[\frac{1-\theta_\mathrm{H}}{1-\theta_\mathrm{H}^0}\exp\frac{(1-\alpha_\mathrm{H})\eta F}{RT} - \frac{\theta_\mathrm{H}}{\theta_\mathrm{H}^0}\exp\frac{-\alpha_\mathrm{H}\eta F}{RT}\right]$ (iii)	$\frac{2.3RT}{(1-\alpha_\mathrm{H})F}$ (for $\theta_\mathrm{H} \approx$ constant)	$-\frac{2.3RT}{\alpha_\mathrm{H}F}$ (for $\theta_\mathrm{H} \approx$ constant)
Volmer–Tafel or Volmer–Heyrovsky	Diffusion (E)	$\eta = \frac{RT}{2F}\ln\left(1 - \frac{i}{i_{\mathrm{l,c}}}\right) - \frac{RT}{2F}\ln\left(1 - \frac{i}{i_{\mathrm{l,a}}}\right)$ (iv)	$\frac{2.3RT}{2F}$	$-\frac{2.3RT}{2F}$

[a] Concentration polarization is neglected in all cases except for (E).

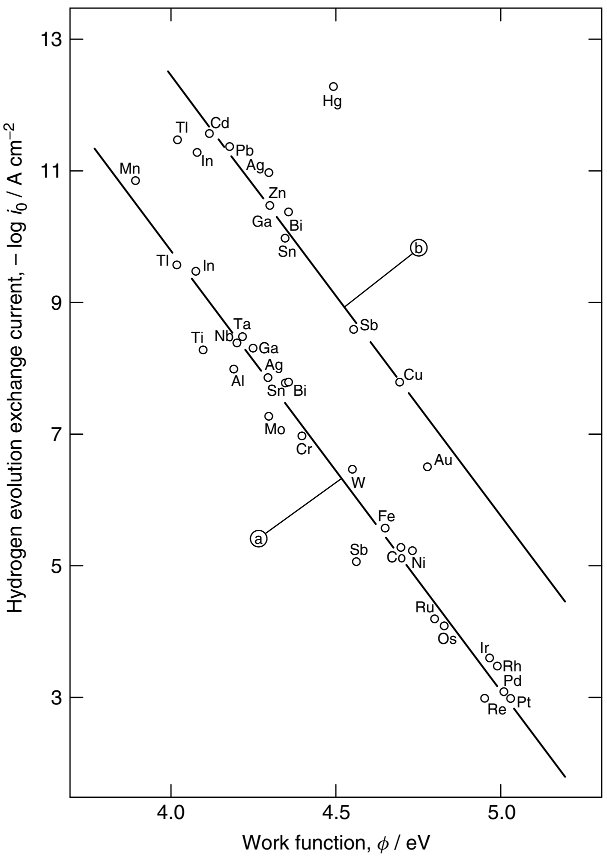

Fig. 9 Exchange current densities for the HER vs. work functions of metals: (a) corresponds to transition metals and sp metals with positively charged surfaces and (b) refers to sp metals with negatively charged surfaces. Reproduced with permission from Ref. [79].

while, however, until the theoretically predicted volcano relationship was confirmed experimentally. The critical aspect is the source for M−H bond energies. Most often reproduced (although not always acknowledged as such) is the volcano relationship between $\log i_0$ and the heat of adsorption of hydrogen on metals as derived by Krishtalik [82] from experimental data for electrochemical hydrogen evolution [79]. However, as pointed out by Trasatti [79], the significance of a volcano plot would have been much greater if the electrochemical data could be correlated with independently measured heats of hydrogen adsorption in the gas phase. This has been done for transition metals [79]. However, for sp metals, which adsorb hydrogen rather poorly, data for hydrogen adsorption in the gas phase are generally not available. Hence the heat of formation of metal hydrides was taken as a measure. Such a volcano plot is presented in Fig. 10. Data for sp and transition metals are shifted with respect to each other along the x-axis. The shift is attributed to the fact that the values for M−H bond energies derived from heats of bulk hydride formation are generally about 20 kcal mol^{-1} (1 kcal = 4.184 kJ) higher than those obtained from adsorption heats. For further details the reader is referred to Refs. [79, 83]. Although the qualitative validity of volcano plots for the HOR/HER is beyond any doubt, quantitative correlations between the exchange current densities and the M−H bond energies must be verified in view of limited experimental data for well-characterized metal surfaces (see the discussion in Ref. [72]).

In agreement with the discussion in Section 8.1.1.4.1, it has been found that for the metals on the ascending branch of the volcano plot, the RDS is associated with the slow discharge reaction (64), whereas for those on the descending branch slow hydrogen atom removal in reaction (63) or (65) is usually the RDS. More precisely, mechanism C (see Table 1) is usually proposed for Pb, Tl, Hg, Cd, Ag, Au and Cu, mechanism D for W, Mo and Nb and mechanism B for platinum metals at low overpotentials; at high overpotentials, some authors proposed for Pt the Volmer–Heyrovsky mechanism (see the discussion in Ref. [68]). It should also be noted that the mechanism of the HER is strongly influenced by the electrode pretreatment and the reaction conditions (potential, pH, temperature, electrolyte composition, etc. [72, 73]). Pt possesses the highest catalytic activity and both HER and HOR on Pt and other platinum metals exhibit high current densities in the vicinity of the equilibrium potential. The activities of Pt electrodes in acidic electrolyte considerably exceed those observed in alkaline solutions. Different explanations have been offered to account for this fact [67, 83], a very likely one being competitive adsorption of OH and H. In practical applications, for water electrolysis massive noble metal electrodes are too expensive to justify their utilization. In alkaline electrolytes, nickel is a reasonable alternative due to its high electrocatalytic activity and stability. Even more suited for industrial electrolysis is steel [68].

The HOR proceeds through the same series of reaction steps as the HER, but in the reverse direction. As already mentioned, the interest in the HOR has greatly increased recently due to the research in the area of low-temperature fuel cells, in particular PEMFCs. Experimental investigations of the HOR in aqueous electrolytes are complicated by mass transport limitation of H_2 due to its low solubility in water ($\sim 10^{-3}$ mol L^{-1}). This problem can be attenuated either by application of a high-speed rotating disk electrode (RDE) [84, 85] or impedance spectroscopy (IS) ([83] and references therein). The HOR has been investigated on noble metal electrodes, most extensively on Pt, and has proven to be structure sensitive and to differ markedly depending on the crystallographic orientation of Pt single-crystal

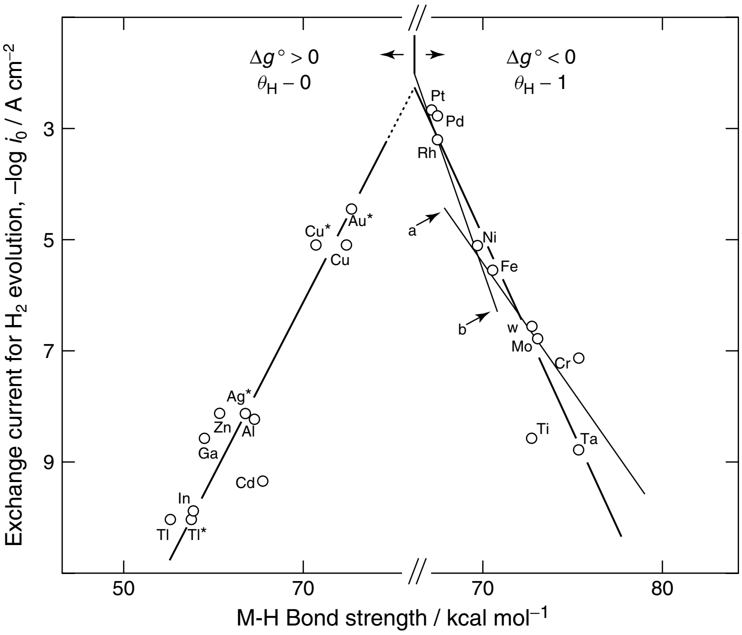

Fig. 10 Exchange current densities for the HER vs. strength of M—H bond derived from the heat of hydride formation in the case of sp metals and from the heat of hydrogen adsorption from the gas phase in the case of transition metals. Reproduced with permission from Ref. [79].

surfaces [83, 84]. No agreement has been achieved so far concerning the particle size effects in the HOR/HER (see discussion in Ref. [83]).

The oxidation of H_2 is strongly suppressed when CO impurities are contained in the hydrogen stream. This is illustrated in Fig. 11, which shows the current–voltage characteristic of a fuel cell fed by pure and CO-contaminated hydrogen. The decrease in the cell performance is due to the fact that CO is strongly adsorbed and blocks surface sites, since CO_{ad} is not oxidized on Pt in the potential interval relevant for the operation of PEMFC anodes. Much attention has been drawn to the search for CO-tolerant anodes for the hydrogen oxidation in view of the development of low-temperature fuel cells fed by reformate gas. Figure 11 shows considerable improvement of the cell performance when PtRu alloys are used at the anode instead of Pt. However, despite substantial improvements, the cell performance in the presence of CO (even with a PtRu anode) does not reach the level achieved with pure hydrogen. The development of CO-tolerant anodes continues to be an active research area; for more information the reader is referred to Refs. [67, 86].

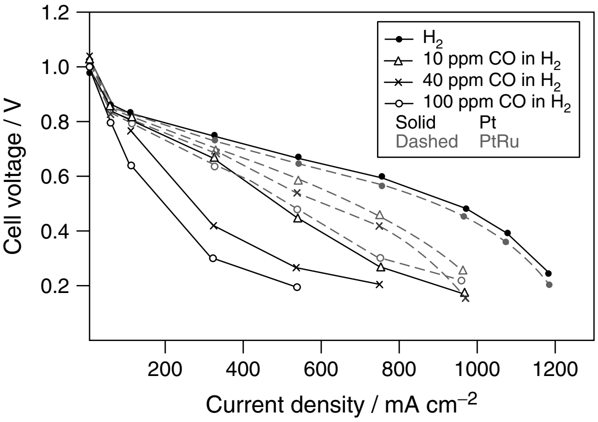

Fig. 11 Influence of CO poisoning in a PEMFC with pure Pt (solid lines) and $Pt_{0.5}Ru_{0.5}$ alloy anodes (dashed lines). The anodes were prepared from 20 wt.% Pt/Vulcan XC72R or 20 wt.% Pt+10 wt.% Ru/Vulcan XC72R at a loading of 0.25 mg Pt cm^{-2}. The cathode uses 40 wt.% Pt/Vulcan XC72R at a loading of 0.6 mg Pt cm^{-2}. The membrane–electrode assemblies (MEAs) are based on catalyzed substrates bonded to Nafion NE-115 membrane. The Ballard Mark 5E single cell is operated at 80 °C with full internal membrane humidification. Reproduced with permission from Ref. [86].

8.1.1.5.3 **Hydrogen Adsorption on Electrode Surfaces**

As already pointed out, the formation of chemisorbed hydrogen is of paramount importance in the overall mechanism of both the HER and the HOR. Electrochemical adsorption of hydrogen has been extensively studied on noble metal electrodes (for references see, e.g., Ref. [71]). It occurs via the discharge of protons in acidic or the reduction of water molecules in basic medium. The phenomenon of the so-called "underpotential deposition" (UPD) of hydrogen was first recognized (although not yet designated as such) by Frumkin and Slygin [87] when they analyzed charging curves on Pt. The term comes from the fact that hydrogen adsorption occurs positive of the reversible potential of the hydrogen electrode. The reaction is strongly sensitive to the electrode material and surface crystallography. Cyclic voltammograms (CVs) for well-ordered low index Pt(*hkl*) single crystals were first reported by Clavilier et al. [88, 89] and are presented in Fig. 12 for the so-called "H_{UPD} region", i.e. the potential region in which UPD of hydrogen occurs. The negative currents in the CVs stem from the discharge of hydronium ions and formation of H_{ad}, while the positive currents are due to the reverse reaction of H_{ad} oxidation.

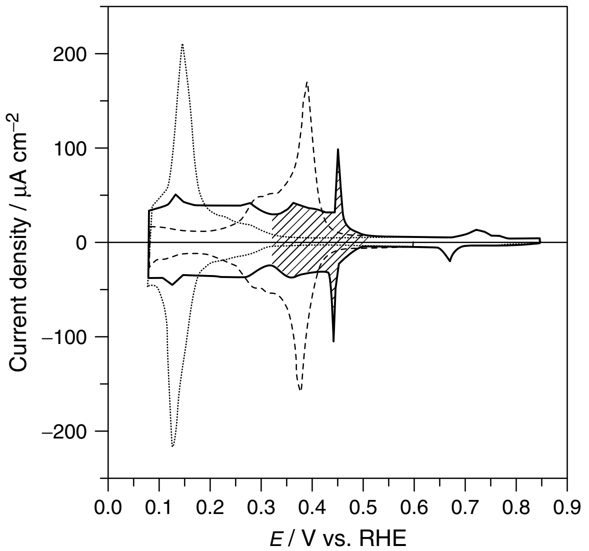

Fig. 12 Cyclic voltammograms for Pt(*hkl*) in H_2SO_4: (111), solid lines; (100), dashed lines; (110), dotted lines. Reproduced with permission from Ref. [83].

Numerous attempts have been made to correlate hydrogen UPD at solid/electrolyte to hydrogen adsorption at solid/gas interfaces. Figure 13 compares H_{UPD} formation and removal on the high index plane Pt(533) from 0.5 M H_2SO_4 with temperature-programmed desorption (TPD) data for the same surface. This surface consists of four-atom-wide terraces of (111) structure separated by (100) steps. One may note striking similarities between the electrochemical and gas-phase data. The high-temperature peak (corresponding to so-called strongly adsorbed hydrogen) in TPD is attributed to hydrogen recombinative desorption from the (100) step sites whereas the low-temperature peak (corresponding to weakly adsorbed hydrogen) stems from H_2 desorption from the (111) terraces [90]. For Pt(111), the high-temperature TPD peak is absent and only the low-temperature peak remains [91]. Analogously, in the electrochemical environment strongly adsorbed hydrogen (above 0.25 V) is attributed to H_{UPD} on (100) sites (cf. Figs. 12 and 13) and the peaks in the interval from 0.1 to 0.2 V to H_{UPD} from (110) and (111) sites. Hence both H_{UPD} and gas-phase hydrogen adsorption are very sensitive to the surface crystallography. The similarities between hydrogen adsorption at the solid/gas and the solid/electrolyte interface are not only qualitative. Also the energy of M−H bonds calculated, e.g., for Pt(111) from the gas phase [92] and from the electrochemical data are in very good agreement [71].

The energetics of hydrogen electrochemisorption has been accessed by a few research groups [93–95] studying the temperature dependence of H_{UPD}. The determination of $\Delta H_{ad}(H_{UPD})$, $\Delta G_{ad}(H_{UPD})$ and $\Delta S_{ad}(H_{UPD})$ on Pt(111) in different electrolytes revealed that the thermodynamic quantities depend only very weakly on the nature of the electrolyte [95]. The bond energy of

References see page 1902

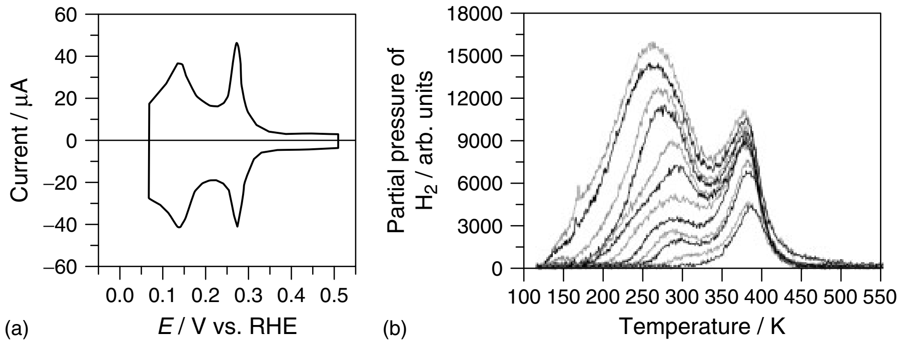

Fig. 13 Comparison of (a) H_{UPD} on Pt(533) in 0.5 M H_2SO_4 measured at 100 mV s^{-1} [171] and (b) thermal desorption spectra of H_2 from the Pt(533) surface. The coverages increase from 0.09 to 0.9. H_2 was dosed at $T_s = 120$ K and the heating rate was 1 K s^{-1}. Reproduced with permission from Ref. [90].

Pt(111)−H_{UPD}, $E_{Pt(111)-H_{UPD}}$, is equal to 262 kJ mol^{-1} at zero coverage [94] (~240 kJ mol^{-1} [95]) and was found to depend only slightly on the hydrogen coverage. The experimental values for $E_{Pt(111)-H_{UPD}}$ are in very good agreement with gas-phase adsorption data ($E_{Pt(111)-H_{UPD}} = 255$ kJ mol^{-1}) [92] and also with the values calculated using DFT ($E_{Pt-H_{ad}} = 252$ kJ mol^{-1} [96]; for more references the reader is referred to Ref. [97]).

Along with the similarities between hydrogen electrochemisorption at solid/liquid and hydrogen chemisorption at solid/gas interfaces, one should consider also the differences which exist between these processes. First, gas-phase hydrogen adsorption involves the dissociation of hydrogen molecules and hydrogen desorption involves the association of hydrogen atoms, whereas H_{UPD} formation or oxidation does not. Instead, the latter processes include highly energetic H^+ solvation or desolvation. The enthalpy of H_3O^+ formation is −754 kJ mol^{-1}; hydration of H_3O^+ to $H_9O_4^+$ releases an additional enthalpy of −356 kJ mol^{-1} [71]. Second, in contrast to hydrogen chemisorption, H_{UPD} formation/oxidation is associated with a charge transfer and thus depends on the electrode potential. Also, the presence of ions may influence H_{UPD}. Indeed, for Pt single-crystal surfaces in sulfuric acid solutions, (bi)sulfate adsorption is superimposed on H_{UPD}. The two adsorption processes are clearly resolved in the CV of Pt(111) in H_2SO_4 electrolyte: the low-potential contribution is related to H_{UPD}, whereas the high-potential component is due to chemisorption of (bi)sulfate (see hatched part in Fig. 12). On Pt(111) in H_2SO_4 the maximum H_{UPD} coverage amounts to 0.66, whereas that of sulfate/bisulfate is 0.21 [98]. In alkaline electrolytes, H competes for the adsorption sites with OH.

One of the main goals in electrocatalysis is to establish relationships between the structure and the electronic properties of an electrode material and its chemisorptive and catalytic properties. It has recently been shown by DFT calculations that the electronic properties of a surface can be modified considerably by changing nearest-neighbor separations through the formation of pseudomorphic overlayers on foreign substrates [99, 100]. This theoretical prediction has been verified experimentally by a number of research groups. For example, Kibler et al. [101] observed a systematic shift of the H_{UPD} peak on pseudomorphic Pd monolayers on different substrates of (111) orientation (Fig. 14a). The position of the H_{UPD} peak correlated with the d-band center $\delta\varepsilon_d$ calculated using DFT (Fig. 14b) [100].

The formation of UPD hydrogen positive of the hydrogen reversible potential is a unique property of noble metal electrodes. However, adsorbed hydrogen is formed on all metal electrodes evolving hydrogen as an intermediate in reactions (63)–(65). In order to make a distinction between these two types of chemisorbed hydrogen at the solid/electrolyte interface, it was suggested (see, e.g., Refs. [102, 103]) to name the latter overpotentially deposited (OPD) hydrogen. We would like to stress that chemically H_{UPD} and H_{OPD} are identical, but they are believed to differ in terms of adsorption sites and bonding energies. On noble metal electrodes H_{OPD} is assumed to form on top of a H_{UPD} monolayer, but may also form when H_{UPD} is fully suppressed, e.g. by a monolayer of chemisorbed sulfur ([71] and references therein). In contrast to this widely accepted view, Breiter argues ([66] and references therein) that an assumption on the existence of two types of adsorbed hydrogen (H_{OPD} and H_{UPD}) is excessive and that it is H_{UPD} which becomes mobile in the vicinity of a monolayer coverage and participates in the HER/HOR. It has been proposed that in the case of the HOR the H_{UPD} is not a reactive intermediate either. Some authors considered this reactive intermediate as H_{OPD}, which by definition is incorrect since the HOR occurs above the reversible potential of the hydrogen electrode. This semantic problem, however, does not resolve the issue

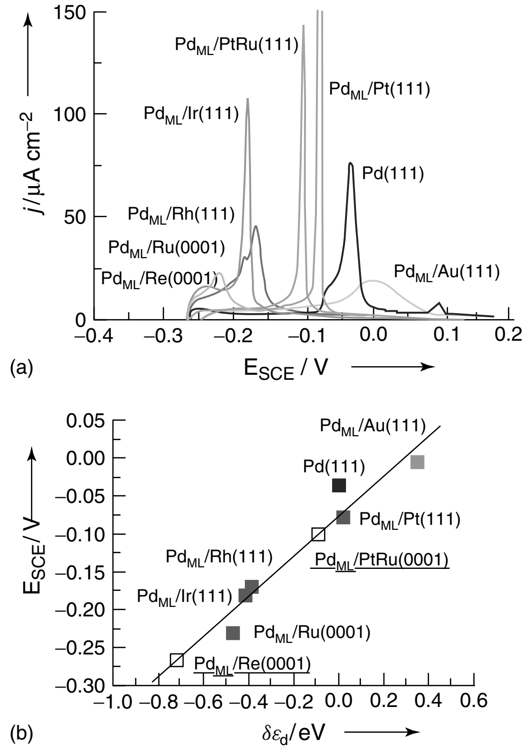

Fig. 14 (a) Positive sweeps of the CVs for Pd(111) and pseudomorphic palladium monolayers (Pd_{ML}) on seven different single-crystal substrates in 0.1 M H_2SO_4, revealing a spectrum for hydrogen desorption. Scan rate, 10 mV s^{-1}. (b) Plot of the hydrogen desorption potentials versus the shift of the d-band center $\delta\varepsilon_d$ (calculated using DFT [100]). Reproduced with permission from Ref. [101].

of the reactive intermediate in the HOR or the HER. Given the experimental data on the RDE curves for H_2 oxidation and recent IR spectroscopic evidence [104], it is indeed likely that the reactive intermediate both in HER and HOR is different from H_{UPD}.

An important issue which has not been fully resolved yet concerns the adsorption sites for H_{UPD} and for the reactive intermediate in HOR/HER. It is usually speculated that H_{UPD} occupies multi-coordinated sites [three-fold sites on (111) and four-fold sites on (100) surfaces], whereas H_{OPD} resides in an atop position (see discussion in Ref. [71] and references therein). However, somewhat conflicting evidence comes from IR/VIS SFG (sum frequency generation) investigations by Tadjeddine et al., which favor mono-coordinated H_{UPD} [105, 106].

Interesting data on the adsorption of hydrogen on platinum have recently been obtained with X-ray absorption spectroscopy (XAS) [107]. Highly dispersed 1.5–2.0-nm Pt particles supported on carbon were studied *in situ* in 0.1 M $HClO_4$ electrolyte with Pt $L_{2,3}$ XAS. The experimental results combined with real-space full multiple scattering calculations on model clusters led the authors to the following conclusions: (i) at low coverage a chemisorbed hydrogen atom is highly mobile and possibly delocalized on the surface, (ii) at higher coverage it localizes into fcc sites and (iii) at very high coverage H is also found in atop sites presumably at or near edges. Further research is needed to sort out the issue of adsorption sites of H_{UPD} and of the reactive intermediate(s) in the HOR/HER [71].

8.1.1.6 The Oxygen Reduction and the Oxygen Evolution Reaction

The oxygen reduction reaction (ORR) and the oxygen evolution reaction (OER) have been studied extensively because of their importance for many practical systems. The OER occurs in water electrolyzers and the ORR in metal–air batteries and fuel cells. The overall reactions involve four electrons:

$$O_2 + 4e^- + 4H^+ \rightleftharpoons 2H_2O \tag{70}$$

with $E^0 = 1.23$ V vs. SHE at 298 K (in acidic electrolytes), and

$$O_2 + 4e^- + 2H_2O \rightleftharpoons 4OH^- \tag{71}$$

with $E^0 = 0.40$ V vs. SHE at 298 K (in alkaline electrolytes).

In contrast to the reactions at the hydrogen electrode, those occurring at the oxygen electrode are characterized by a very sluggish reaction kinetics even at the most catalytically active Pt electrodes, hence a high negative (positive) overpotential is required to reduce (form) O_2 at an appreciable rate. Because of this, cathodic and anodic reactions occur on essentially different electrode surfaces: The ORR takes place on pure or oxygen-covered metal surfaces (depending on the type of metal) whereas the OER proceeds on oxide phases. The exchange current density of the ORR/OER is typically in the range 10^{-9}–10^{-11} A cm^{-2}. Because of these small values, the activities of different electrode materials towards the ORR/OER are usually characterized by current densities at specified electrode potentials rather than by the exchange current densities. The ORR and the OER have been subject of many reviews, e.g. Refs. [108–112]. In Sections 8.1.1.6.1–8.1.1.6.4 we summarize important aspects of the ORR and in Section 8.1.1.6.5 those of the OER, both in aqueous electrolyte solutions. We start our discussion with reaction mechanisms and their relation to the electrode material (Section 8.1.1.6.1). Since the formation of various oxygen-containing species plays a key role in the ORR, Section 8.1.1.6.2 is devoted to water electrochemisorption and molecular oxygen adsorption on noble metal electrodes. In Section 8.1.1.6.3, we briefly discuss structural and particle size effects in the ORR, and Section 8.1.1.6.4 deals with catalyst development for the ORR in polymer electrolyte fuel cells. High-temperature studies of the ORR are not treated below; interested readers are referred to a review paper [113] and references therein. In Section 8.1.1.6.5, the most important aspects of the OER are summarized.

8.1.1.6.1 Reaction Mechanisms: Relation to the Electrode Material

The ORR is a multielectron electrochemical reaction that, depending on the electrode material and the reaction conditions, may involve various reaction intermediates, in particular $O_{2,ad}$, $O^-_{2,ad}$, $HO_{2,ad}$, O_{ad}, OH_{ad}, $H_2O_{2,ad}$. The latter may desorb from the electrode surface and can be detected in the electrolyte. A scheme showing different pathways of the ORR, including the intermediate formation of H_2O_2 was proposed by Wroblowa et al. [114] and Bagotskii et al. [115] and is represented in Fig. 15. The 4 e$^-$ path (k_1)

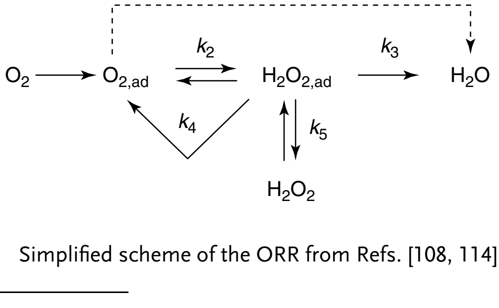

Fig. 15 Simplified scheme of the ORR from Refs. [108, 114].

References see page 1902

is usually termed the *direct* or *parallel* pathway and that involving intermediate H_2O_2 formation the *series* pathway (k_2 and k_3). H_2O_2 may also catalytically decompose on the electrode surface (k_4). Isotope measurements showed that hydrogen peroxide formation occurs without O−O bond splitting (see Ref. [108] and references therein), while water formation obviously requires it. Much research has been directed towards the understanding of the ORR mechanism on various electrode materials. In 1959, Frumkin et al. proposed to use a rotating ring disk electrode (RRDE) [116] for detecting stable intermediates formed at the working electrode in the course of complex electrochemical reactions. Detection of H_2O_2 at the ring electrode gives evidence that the ORR follows the series rather than the direct mechanism. Since 1960, many research groups have put considerable effort into investigating the ORR using RRDE with various disk electrode materials. Details of these studies can be found in review articles [108–111].

According to the mechanism of the ORR, electrode materials can be divided into two groups. The first comprises metals which catalyze the ORR predominantly via the $2e^-$ peroxide mechanism. These include mercury, graphite, gold {except for Au(100) in alkaline solution [117]}, the majority of metal oxides and oxide-covered metals. The ORR was studied most thoroughly on Hg and graphite electrodes in alkaline electrolytes. Two reduction waves were observed and could be assigned unambiguously: the first wave corresponds to the reduction of oxygen to peroxide and the second to the reduction of peroxide to water. Investigations of the reaction orders with respect to molecular oxygen and H^+ suggest that the RDS on Hg and graphite electrodes is the first electron transfer both in the first wave, i.e. O_2 reduction, and in the second wave, i.e. the H_2O_2 reduction reaction.

Predominantly $4e^-$ oxygen reduction occurs on Pt and other platinum metals, and also on Pt-based alloys, Ag and, as already mentioned, Au(100) in alkaline electrolytes. Despite the fact that the ORR has been extensively investigated on Pt metals (especially on Pt), first on polycrystalline and later on single-crystal electrodes [13], there is as yet no consensus regarding the detailed reaction mechanism. For polycrystalline Pt in alkaline electrolytes some H_2O_2 was detected (although in small quantities) at the ring of an RRDE. Hence the series mechanism was proposed. In acidic solutions, the amount of hydrogen peroxide formed is usually lower. The absence of H_2O_2 in the electrolyte, however, does not imply that $H_2O_{2,\text{ad}}$ is not formed as a reaction intermediate. It just means that if it is produced it does not leave the working electrode due to either a high k_3 or a high k_4 value. The Tafel slopes for polycrystalline and for supported Pt nanoparticles in acidic solutions have been found to change from ca. −120 mV decade^{-1} in the potential interval below ca. 0.8 V vs. RHE to ca. −60 mV decade^{-1} at higher electrode potentials. The change in the Tafel slope has been attributed to the fact that below ca. 0.8 V vs. RHE the Pt surface is free from oxides, whereas above 0.8 V it is covered by oxides. Hence understanding the ORR on surfaces adsorbing oxygen and forming surface oxides requires understanding the surface state under relevant conditions.

8.1.1.6.2 Oxygen Adsorption and Formation of Surface Oxides and Their Relation to the ORR

Formation of adsorbed oxygen species and surface oxides may occur on electrode surfaces either by electrochemical adsorption and decomposition of water or via the interaction with molecular oxygen. The electrochemical oxidation of noble and IB metal surfaces has been investigated by numerous electrochemical methods and also by surface-sensitive techniques performed either *in situ* using IR spectroscopy, ellipsometry, electrochemical quartz-crystal microbalance (EQCM), XAS and X-ray scattering, electrochemical scanning tunneling microscopy (STM) and Raman spectroscopy, or *ex situ* with the electrodes removed from the electrochemical cell and transferred to ultra-high vacuum (UHV) using, e.g., X-ray photoelectron spectroscopy (XPS), Auger electron spectroscopy (AES) or STM (see, e.g., review articles [118, 119] and references therein). Whereas the formation of oxide phases on the electrode surfaces has been studied fairly extensively, much less is known about the initial steps of metal oxidation.

The first step of surface oxidation is usually assumed to be OH_{ad} formation, which in acidic and alkaline electrolytes reads

$$\mathrm{M} + \mathrm{H_2O} \rightleftharpoons \mathrm{M} - \mathrm{OH_{ad}} + \mathrm{H}^+ + e^- \qquad (72)$$

$$\mathrm{M} + \mathrm{OH}^- \rightleftharpoons \mathrm{M} - \mathrm{OH_{ad}} + e^- \qquad (73)$$

respectively. This step has a clear voltammetric signature for Pt(111) in alkaline and acidic aqueous electrolytes of weakly adsorbing anions (e.g. $HClO_4$) [13], Au(111) [120] in neutral and alkaline electrolytes and Ag(*hkl*) in alkaline electrolytes [121, 122]. The reversible nature of OH adsorption on Pt(111) is reflected by mirror-like anodic and cathodic peaks. Using density functional theory, Anderson ([123] and references therein) calculated the reversible potential of reaction (72) on Pt to be 0.62 V vs. RHE. The Pt(111)–OH_{ad} bond energy has been estimated as ∼136 kJ mol^{-1} in alkaline electrolyte, which is much smaller than the Pt−O_{ad} bond energy (∼350 kJ mol^{-1}) at a gas/solid interface (see Refs. [13, 95] and references therein for details). In solutions containing strongly adsorbing anions (e.g. SO_4^{2-}), OH adsorption is inhibited by anion chemisorption. Despite the importance of OH_{ad} and O_{ad} for the ORR and the oxidation of CO and other organic molecules, papers reporting their direct spectroscopic observation are scanty. Among spectroscopic methods applied, Raman spectroscopy [124, 125], IR spectroscopy [120], XPS [121, 126] and XAS [127] should be mentioned.

Whereas the onset of OH_{ad} formation is believed to be reversible, at more positive electrode potentials it becomes irreversible. In order to account for the irreversibility observed for Pt and Au electrodes, Angerstein-Kozlowska and Conway ([118] and references therein) proposed the so-called place-exchange mechanism between metal atoms and OH moieties:

$$\mathrm{M - OH_{ad}} \xrightarrow{\text{placeexchange}} \mathrm{(OH - M)_{quasi\ 3D\ lattice}} \qquad (74)$$

It was proposed that the incorporation of OH into the metal lattice is initiated via place exchange. After the OH species have been transformed into O, the subsequent growth of thick metal oxides presumably takes place by field-assisted transfer of metal cations through this film, into the 3D-type layer via the Mott–Cabrera field-assisted growth mechanism [128]. In more recent investigations, Birss et al. [129] and then Jerkiewicz et al. [130] questioned the above mechanism for Pt electrodes. Through combined cyclic voltammetry, EQCM and Auger electron spectroscopy measurements, Jerkiewicz et al. proposed that the oxidation of Pt surfaces occurs via the formation and subsequent place exchange of O_{ad} rather than OH_{ad} [130].

An essential question is whether the electrochemically formed oxides are equivalent to those formed through gas-phase metal oxidation. This issue has been addressed by Weaver's group in a series of publications ([131] and references therein). Five Pt-group metals, namely platinum, palladium, iridium, rhodium and ruthenium, were examined by means of surface-enhanced Raman spectroscopy (SERS) in aqueous electrochemical and gaseous dioxygen environments as a function of electrode potential and temperature, respectively, with the objective of comparing systematically the conditions required for surface oxide formation and of elucidating the reaction mechanisms involved. In order to obtain surface enhancement, noble metal films were deposited on roughened Au templates. Figure 16 compares SERS spectra of 1–3 monolayers of oxides grown on the surface of a Pt film. Essentially the same band at 575 cm^{-1} develops, in the electrochemical environment above 0.6 V SCE and in the gas-phase environment at 200 °C. It coincides with the wavenumber characteristic of Pt—O stretch previously observed for bulk amorphous PtO_2 [132]. Remarkable is the fact that electrode potential reversal recovers the pristine Pt surface, whereas the gas-phase Pt oxide reduction is kinetically hindered. It was therefore concluded that the oxides formed on noble metal surfaces at solid/liquid and solid/gas interfaces were largely similar (although distinct differences were observed for Pd and Ru). However, the kinetics of their formation and reduction are significantly different: they occur through direct oxide formation at the gas/metal interface and a metal–oxygen place-exchange mechanism, expedited by interfacial solvation in the electrochemical environment. Thus, oxide formation in the anhydrous gas-phase environment is energetically unfavorable.

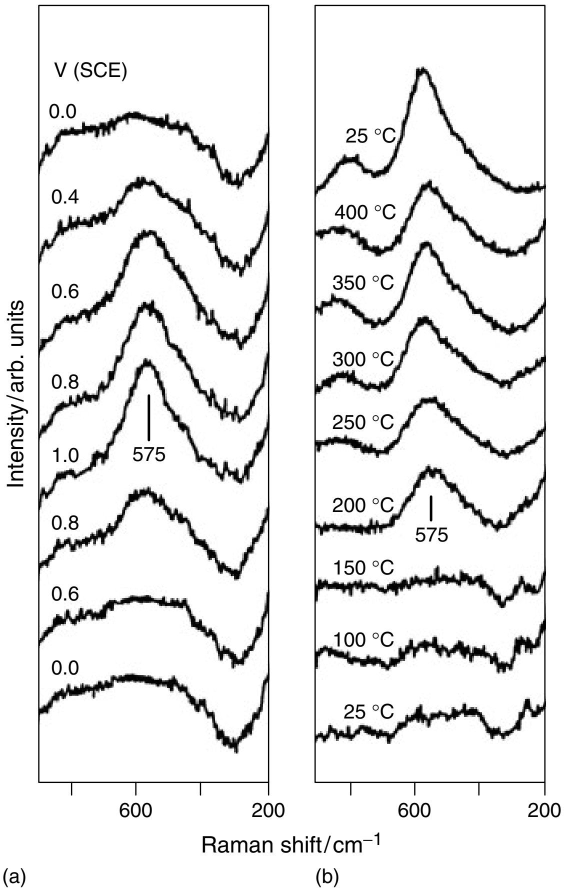

Fig. 16 (a) Potential-dependent SER spectra acquired for electrochemical oxidation and subsequent reduction of a platinum film deposited on an Au substrate in 0.1 M $HClO_4$. The initial potential was 0 V vs. SCE (bottom spectrum), followed by potential increments of 0.2 V up to 1.0 V and finally returning to 0 V. (b) Temperature-dependent SER spectra acquired for thermal oxidation of a platinum film in 1 atm of flowing O_2. The temperature was increased in 50 °C increments before decreasing back to 25 °C. Reproduced with permission from Ref. [131].

Among other techniques utilized for the investigation of metal oxidation, XAS, which allows *in situ* monitoring of structural transformations at the surfaces of both smooth and dispersed metals, can be mentioned. Figure 17

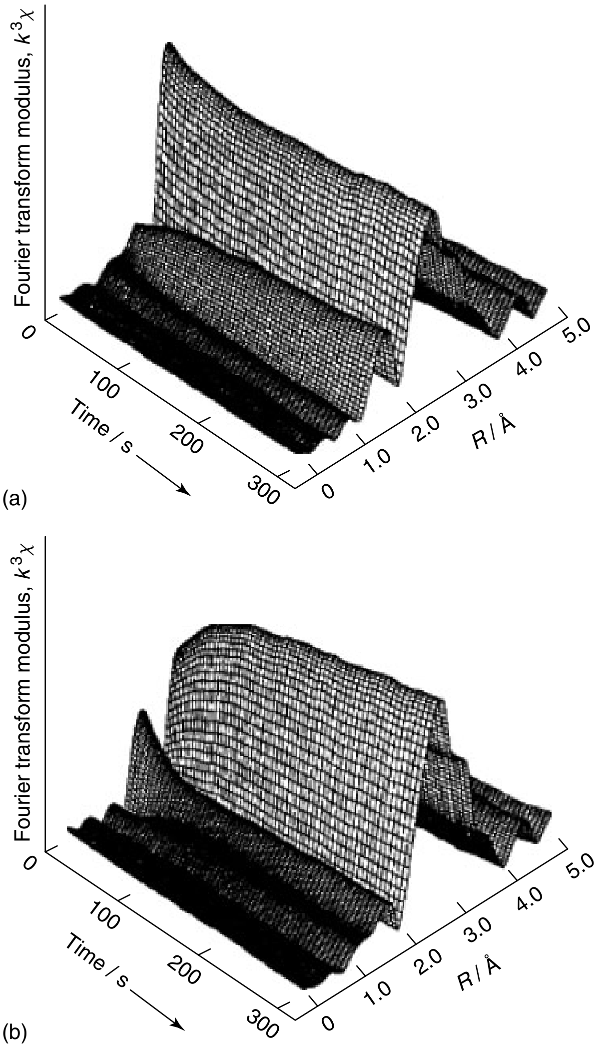

Fig. 17 Fourier transform moduli of the Pt EXAFS ($k = 2.2 - 9.7$ Å^{-1}) acquired during (a) the oxidation and (b) the reduction of Pt/C catalyst (particle diameter ca. 2 nm) as a function of time after jumping the electrode from 0.1 to 1.2 V. The peak at 2.24 Å corresponds to the first shell of Pt near neighbors at 2.76 Å. The peak at 1.50 Å is a combination of the side-lobe from the Pt shell and a shell of O near neighbors at 2.01 Å [133].

shows Fourier transform moduli (describing the radial distribution function around Pt atoms) extracted from Pt L_3 edge EXAFS spectra of carbon-supported Pt nanoparticles measured in the dispersive mode [133]. The catalyst was incorporated in a polymer electrolyte membrane fuel cell operating at 80 °C with 1 atm (101 kPa) of water-saturated N_2 over the working electrode and H_2 on the counter electrode. The appearance and the concomitant growth of the peak corresponding to the Pt−O bond occurred simultaneously with the decrease in the intensity of the peak corresponding to Pt−Pt bond. It was concluded that Pt surface oxidation is accompanied by surface restructuring. Interestingly, in their studies of oxide formation and reduction kinetics, the authors did not find a signature of the place-exchange mechanism proposed for smooth surfaces. Overall we would like to stress that the structure and dynamics of the interface under conditions relevant for the ORR and other electrocatalytic reactions is a key issue of modern electrocatalysis and further studies are necessary to achieve a better understanding.

As already mentioned, surface oxides formed on Pt and other metal electrode surfaces strongly influence the kinetics and mechanism of the ORR. The change in the Tafel slope observed for polycrystalline Pt electrodes during the ORR has been attributed to the build-up of Pt oxides on the electrode surface above 0.8 V vs. RHE [134]. The apparent coverage of electrodes by oxygen-containing species determined from the charge has been found to increase linearly with the electrode potential.

For polycrystalline Pt, the reaction order with respect to oxygen is 1 in both potential intervals (below and above 0.8 V vs. RHE), whereas the reaction order with respect to protons changes from 1 in the low-potential region to ca. 1.67 in the high-potential region [134]. These results were interpreted in terms of the addition of the first electron to the adsorbed oxygen molecule as the RDS:

$$O_2 + H^+ + e^- \longrightarrow O_2H_{ad} \qquad (75)$$

For the oxide-free surface this agrees well with a -120 mV decade^{-1} Tafel slope for $\alpha = 0.5$. For partially oxide-covered surfaces, assuming that the free energy of activation for the ORR depends on the coverage of the surface oxide, a change in the Tafel slope to -60 mV decade^{-1} can be predicted, which is in agreement with the experimental data. The relevance of water electrochemisorption to the change in the Tafel slope has recently been confirmed by varying the content of water in the electrolyte [135]. The experiments were performed in H_2O−TFMSA (trifluoromethanesulfonic acid) mixtures with the water:acid mole ratio varied from 50 : 1 to 4 : 1. Whereas at high water contents the Tafel slope changed from -112 to -59 mV decade^{-1} in agreement with what has been observed previously in aqueous solutions of H_2SO_4 and $HClO_4$, at low water contents no change in the Tafel slope was observed (Fig. 18). This substantiates the involvement of water in the formation of oxides on the Pt surface.

One of the critical issues is related to whether the adsorbates formed through dissociative adsorption of molecular oxygen are equivalent to those formed via water electrochemisorption. Yeager [136] suggested that the mechanism of the ORR depends on the type of molecular oxygen bonding to the electrode surface. Three models for molecular oxygen bonding have been

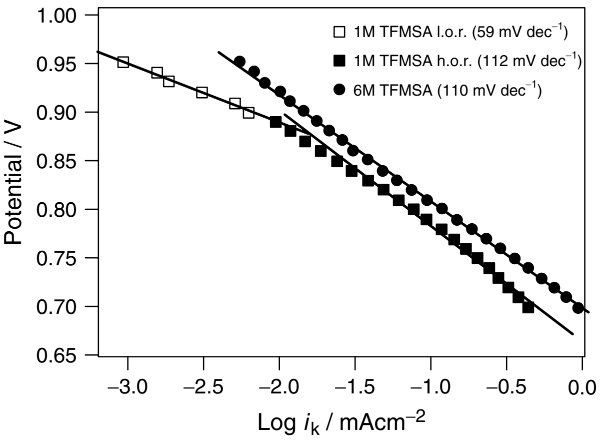

Fig. 18 Tafel plots for the ORR at room temperature on a polycrystalline Pt bulk electrode at 1225 rpm based on the potential sweep from 1.2 to 0.3 V at 25 mV s^{-1} in 1 and 6 M CF_3SO_3H. Reproduced with permission from Ref. [135].

proposed: (a) according to the Griffith model [137], an O_2 molecule interacts with a single substrate atom by forming a bond between its π orbitals and the empty d_z^2 orbitals of the metal surface atom; (b) in the end-on Pauling model [138], the σ orbital of an O_2 molecule donates electron density to an acceptor d_z^2 orbital of the metal; (c) the bridge model holds if an oxygen molecule binds to two surface atoms. Yeager [136] suggested that type (a) and (c) adsorption of oxygen favors O—O bond splitting and thus the direct 4e path of the ORR, whereas type (b) adsorption results in the 2e pathway of the ORR and the formation of H_2O_2. To gain further information on the type of O_2 adsorption during the ORR, Adzic and Wang [139] used the adsorption of foreign (Ag) adatoms to probe the oxygen adsorption reaction at a Pt(111) surface. The inhibition of the ORR on Pt(111) by sub- and monolayer coverages of Ag was studied using electrochemical and *in situ* surface X-ray scattering techniques. The analysis of the extent of the inhibition of the ORR as a function of the Ag coverage showed that the data are best interpreted with O_2 adsorbed at a bridge site.

Oxygen adsorption on Pt surfaces from the gas phase has been studied with many spectroscopic techniques with the aim of identifying and characterizing different adsorption states. O_2 is physisorbed on Pt(111) below 90 K; at higher temperatures two chemisorbed molecular states have been identified, superoxo (O_2^-) and peroxo (O_2^{2-}), with different extents of electron donation from the Pt surface to the oxygen molecule. It was demonstrated that the two chemisorbed molecular states have O_2 lying on bridging di-σ and $\mu - \pi$ sites. Above 150 K O_2 dissociates to form atomically adsorbed oxygen in 3-fold hollow surface sites. For references the reader is referred to Ref. [140].

Recently, the ORR has attracted the close attention of theoreticians who performed quantum chemical calculations of reaction intermediates using different computational approaches [29, 140–146]. Potential energy surface profiles for the 2e and 4e O_2 reduction on Pt have been considered, the 4e path being identified as the dominant one [144, 145, 147]. Anderson et al. considered both end-on adsorption of O_2 to a single Pt atom [148] and a bridge-bonded O_2 molecule adsorbed to a Pt_2 cluster [140]. In agreement with the earlier hypothesis of Yeager, it was concluded that oxygen bonding to a single Pt atom would result predominantly in H_2O_2 formation, whereas bridge-bonding O_2 favors 4e reduction. Comparison of the activation barriers for different reaction intermediates suggests that O_2 dissociation does not occur before electron and proton transfer, which greatly diminish the activation barrier for O—O bond splitting. The first electron transfer step was identified as the RDS and its activation energy at the reversible electrode potential was estimated as 0.60 [140] to 0.5 eV [149], which is close to the experimental value of 0.44 eV on Pt(111) in H_2SO_4 [150]. Electric field dependences of adsorbates on Pt(111) have been calculated [146]. Lowering the field causes an increase in the O—O bond length of O_{2ad}^-, attracting the molecule to the Pt surface and increasing the charge transfer from Pt to $2\pi^*$ orbitals of the oxygen molecule.

8.1.1.6.3 Structural and Particle Size Effects in the ORR

An influence of surface crystallography on the kinetics and the mechanism of the ORR has been observed for different materials. For example, the basal plane of graphite was found to be significantly less active than the edge plane. This has been explained by the lack of adsorption sites for O_2, O_2^- and HO_2^- on the basal plane. In contrast, on edge planes oxygen can adsorb at the edges of graphene layers [108, 110, 151, 152]. Structural effects for Pt(*hkl*) have been investigated by Markovic et al. in both acidic and alkaline electrolytes ([13] and references therein, [153]). In Fig. 19, the significant influence of the crystallographic orientation of Pt on the rate of the ORR (which is proportional to the disk current shown) and the amount of H_2O_2 formed (for which the ring current is a measure) can be seen. The order of activity of Pt(*hkl*) in 0.1 M KOH increased in the sequence (100) < (110) < (111) for both oxygen and peroxide reduction. These differences were attributed to the structure sensitivity of hydroxyl anion (OH^-) adsorption on Pt(*hkl*) and its inhibiting (site-blocking) effect on oxygen kinetics. In recent studies, Wang et al. [154] proposed that along with site-blocking effects,

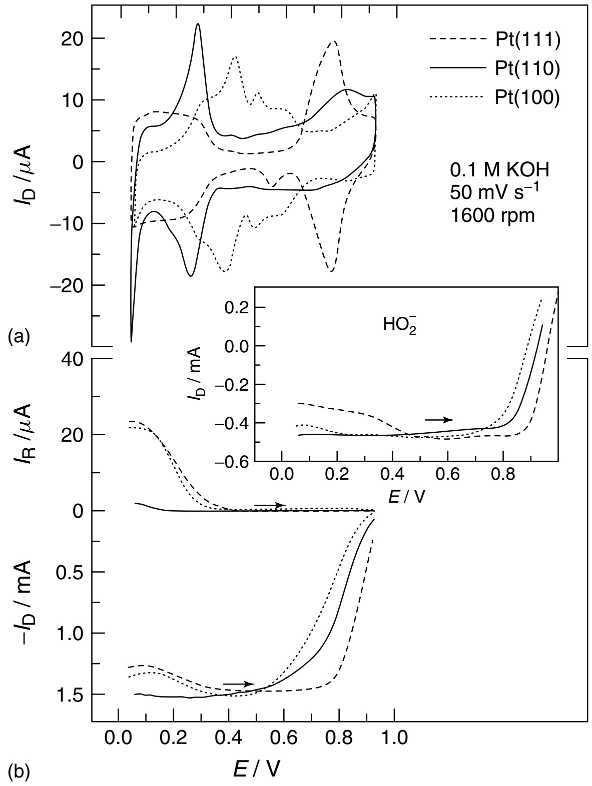

Fig. 19 (a) Cyclic voltammetry of Pt(*hkl*) in oxygen-free 0.1 M KOH electrolyte in the RRDE assembly. (b) Disk (I_D) and ring (I_R) currents during ORR on Pt(*hkl*) (ring potential 1.15 V). Insert: reduction of HO_2^- on Pt(*hkl*) mounted in the RRDE assembly; 0.1 M KOH, 50 mV s^{-1}, 1600 rpm. Reproduced with permission from Ref. [172].

anions also exert electronic effects on the ORR. The mechanism of O_2 reduction is also affected by adsorbed hydrogen, with the increased formation of peroxide ions in the H_{UPD} region. Adsorbed hydrogen has an inhibiting effect on peroxide reduction, the effect decreasing in the order (111) > (100) ≫ (110).

Particle size effects were discovered for the ORR on Pt nanoparticles in phosphoric acid many years ago in connection with the development of cathode catalysts for phosphoric acid fuel cells (PAFCs) ([110, 155] and references therein). Similar dependences have been reported more recently also in electrolytes containing weakly adsorbing anions, such as in $HClO_4$ [156]. The specific electrocatalytic activities were found to decrease substantially with increase in the Pt specific surface area (corresponding to a decrease in the particle size) (Fig. 20). Different hypotheses have been proposed to account for this negative particle size effect. According to Kinoshita [157, 158] and Mukerjee [159], the size effect ensues from different fractions of (100), (111) and (110) sites on particles with different sizes. Gasteiger et al. [156] attributed the negative particle size effect to an increase in the strength of OH adsorption (and thus surface blocking) with decreasing particle size. An alternative viewpoint was presented by Stonehart and Watanabe (see discussion in Ref. [159]), who proposed that the apparent correlation between the catalytic activity of nanoparticles and the particle sizes stems from interparticle diffusive interference between the platinum crystallites. This interpretation is based on the observation that the specific activities of platinum particles of different sizes became identical on different carbon supports when the crystallite separations on the carbon supports were similar. Further studies are needed to understand better the influence of particle sizes on the electrocatalysis of the ORR.

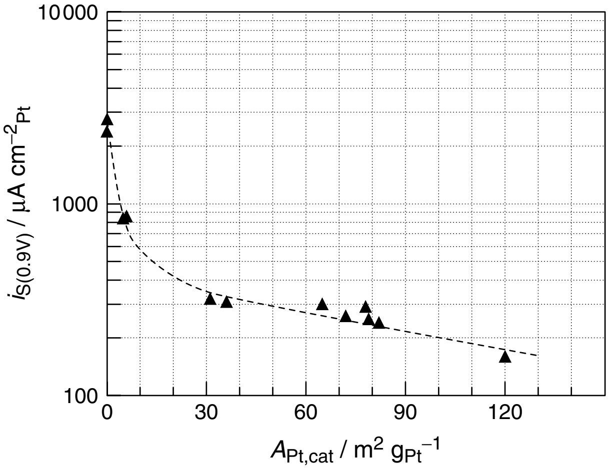

Fig. 20 ORR specific activities for Pt/C catalysts, polycrystalline Pt (shown at 0 m^2 g^{-1}) and Pt black (at 5 m^2 g^{-1}) at 0.9 V vs. RHE in 0.1 M $HClO_4$ at 60 °C as a function of their specific surface areas. Reproduced with permission from Ref. [156].

8.1.1.6.4 ORR Electrocatalysis for Low-Temperature Fuel Cells

The ORR occurs at the cathode of both low- and high-temperature fuel cells and its sluggish kinetics is greatly responsible for the fact that the cell voltage V_{cell} is much below the equilibrium value of the H_2/O_2 cell ΔE_{eq} (which depends on the temperature and the gas partial pressures). This is illustrated in Fig. 21.

The cell voltage can be expressed as follows (see also Section 8.1.1.2.3):

$$V_{cell} = \Delta E_{eq} - |\eta^*_{ORR}| - |\eta_{HOR}| - \Delta E_{ohmic} \qquad (76)$$

where η^*_{ORR} and η_{HOR} represent the overpotentials at the cathode and the anode, respectively. In a fuel cell fed by pure hydrogen η_{HOR} is small and is often neglected [156]. η^*_{ORR} can be separated into the reaction overpotential η_{ORR} and concentration overpotential η_{conc}. The former is the consequence of the intrinsically sluggish ORR

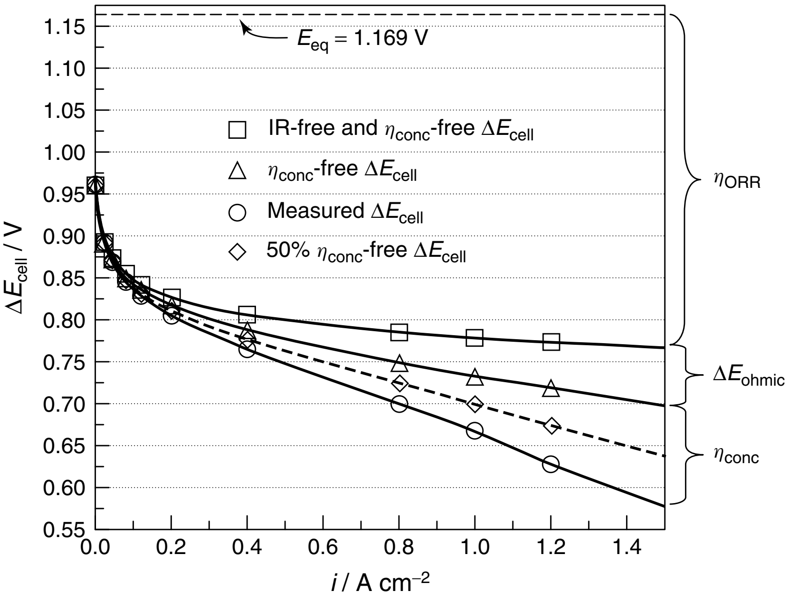

Fig. 21 Current–voltage characteristic obtained in a 50 cm^2 hydrogen–air fuel cell at 80 °C at a total pressure of 150 kPa. The anode and cathode layers consist of ca. 50 wt.% Pt/carbon [0.4/0.4 mg Pt cm^{-2} (anode/cathode)] and ionomer (ca. 900 EW; ionomer:carbon ratio = 0.8 : 1). Circles, experimental data; triangles, mass transport-free E_{cell}; squares, mass transport-free and ohmically corrected E_{cell}. The current density is referred to the geometric surface area of the MEA. Reproduced with permission from Ref. [156].

kinetics discussed above, whereas the latter arises from the oxygen mass transport limitations in the catalytic layer. ΔE_{ohmic} comprises the contributions of (i) the contact resistance between the flowfield plates, (ii) the membrane resistance and (iii) the resistance of the catalytic layers and the diffusion layers. ΔE_{ohmic} can be measured directly via either current-interrupt or high-frequency resistance measurements. Since the electrochemical fuel cell efficiency is given by the ratio between V_{cell} and ΔE_{eq}, Eq. (76) and Fig. 21 give a guidance to which contributions must be minimized in order to improve the fuel cell efficiency. As is apparent from Fig. 21, at low current densities the difference between the actual cell voltage and the thermodynamic equilibrium value is fully determined by the cathode overpotential (η_{ORR}). At high current densities, mass transport of oxygen to the active centers and ohmic losses also make significant contributions to the overall losses. ΔE_{ohmic} can be decreased by utilizing polymer membranes with higher ionic conductivities and optimization of the operation conditions. However, ohmic losses in other cell components such as bipolar plates and catalytic layers must also be minimized. η_{conc} depends hugely on the architecture of the catalytic layers and porosities of catalytic supports utilized. Since the main losses come from η_{ORR}, much effort has been directed towards the development of novel electrode materials for PEMFC applications. Here, the goal is to maximize the electrocatalytic activity while decreasing the amount of precious metals.

Pt alloys (such as PtCr, PtNi, PtCo and PtFe and also ternary alloys) show noticeable enhancement of the ORR activity both in PAFC and PEMFC [156, 159]. Different hypotheses have been offered to account for the enhanced electrocatalytic activity of Pt alloys with transition metals [156]. However, most authors nowadays agree that the enhanced ORR kinetics can be explained by an electronic effect of the transition metals, which results in the inhibition of OH adsorption on Pt [135, 160]. This is supported by *in situ* EXAFS results [135] and by quantum chemical calculations [161].

Another approach towards the improvement of cathode catalysts for PEMFCs, first proposed by Brankovic et al. [162], utilizes Pt monolayers on foreign metal nanoparticles. This allows (i) the electrocatalytic activity of Pt to be tuned by inducing lattice strain and (ii) the amount of Pt per unit current density to be decreased significantly. Electrocatalysis of the ORR on Pt monolayers supported on nanoparticulate and single-crystal electrodes has been considered extensively by several research groups (see, e.g., Ref. [163] and references therein). For example, in Fig. 22 the electrocatalytic activities of platinum monolayers on Ru(0001), Ir(111), Rh(111), Au(111) and Pd(111) towards the ORR are compared. A strong influence of the substrate on both the reduction current and the amount of H_2O_2 produced can be observed. In this context, it should be mentioned that

References see page 1902

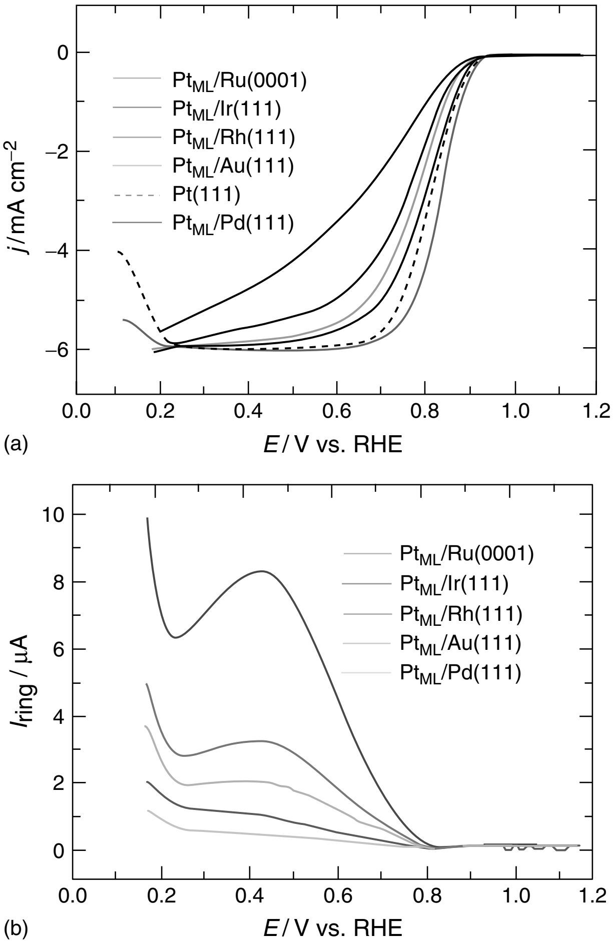

Fig. 22 Disc (a) and ring (b) currents for the ORR at the RRDE on platinum monolayers (PtML) on Ru(0001), Ir(111), Rh(111), Au(111), Pd(111) and for Pt(111) electrode in 0.1 M $HClO_4$ solution. The rotation rate is 1600 rpm and the sweep rate is 20 mV s^{-1} [50 mV s^{-1} for Pt(111)]. The ring potential is 1.1 V and the collection efficiency is 0.20. The electrode labelling: from left to right (a) and from top to bottom (b). Reproduced with permission from Ref. [143].

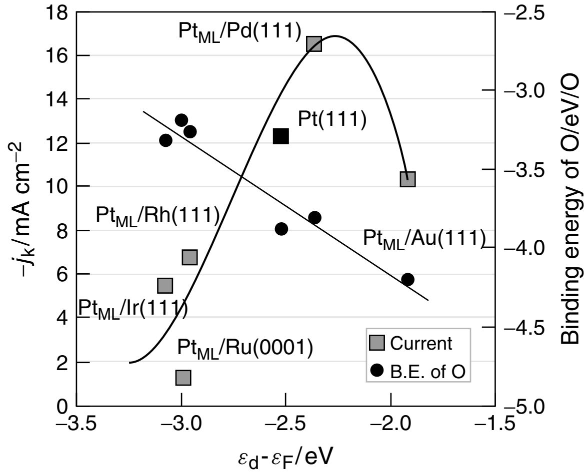

Fig. 23 Kinetic currents (j_K; squares) at 0.8 V for O_2 reduction on platinum monolayers supported on different single-crystal surfaces in 0.1 M $HClO_4$ solution and calculated binding energies of atomic oxygen (BEO; filled circles) as functions of calculated d-band center relative to the Fermi level of the respective clean platinum monolayers. The current data for Pt(111) are included for comparison. Reproduced with permission from Ref. [143].

in terms of the development of PEM fuel cells it is necessary to obtain cathode materials catalyzing 4e oxygen reduction, since hydrogen peroxide production not only decreases the efficiency of a cell, but also leads to the degradation of the cell components, in particular polymer membranes.

The platinum monolayers on Ru(0001), Rh(111) and Ir(111) are compressed compared with Pt(111), whereas on Au(111) it is stretched by more than 4%. DFT studies have shown that compressive strain tends to downshift the weighted center of the d-band whereas tensile strain has the opposite effect [164]. The experimentally determined kinetic currents (corrected for the mass transport effects) show a volcano-type dependence on the center of their d-bands as determined by DFT calculations (Fig. 23) [143]. The platinum monolayer supported on Pd(111) is at the top of the volcano curve and shows improved ORR activity over pure Pt(111). The oxygen binding energy to the surface has also been computed and is plotted in Fig. 23. It has been suggested that the volcano-type behavior is determined by two opposite trends: whereas a higher lying d-band center tends to facilitate O—O bond breaking, a lower lying one tends to facilitate bond formation (hydrogen addition). The results suggest that an improvement in the overall fuel-cell efficiency can be combined with substantial cost savings that result from using less platinum at the cathode. Similar logics can be applied when discussing the behavior of PtM alloys. Along with Pt and Pt alloys, other materials have been investigated in the ORR, in particular metal oxides [165], macrocyclic N4-transition metal chelates [166] and Ru chalcogenide materials [167]. The interested reader should consult the above references.

8.1.1.6.5 **Oxygen Evolution Reaction** The oxygen evolution reaction [the reverse reaction of (70) in acidic and of (71) in alkaline electrolytes] has been investigated on various electrode materials ([73] and references therein). It occurs in the potential interval where metal surfaces are covered by phase oxides. Participation of Pt oxides in the OER was proposed in early isotope experiments of Rosenthal and Veselovski [168]. They covered the Pt electrode surface with surface oxide enriched with ^{18}O. Mass spectrometric analysis of the oxygen evolved on the anode proved its enrichment with ^{18}O.

Although Pt and its alloys are the best catalysts for the ORR, they are not the most active catalysts for the OER. Their poor catalytic activity towards the OER stems in part from the insulating properties of Pt oxides. The best catalysts for the OER are materials which are not only catalytically active but are also conductive and stable. The field of the OER has been reviewed by Kinoshita [110] and will be discussed only briefly here. The ability of an oxide material to change its valence state readily is considered a prerequisite for their high catalytic activity in the OER. Hence it is postulated [110, 112] that the catalytic activity towards the OER is related to the change in enthalpy when the oxide undergoes a transition from a lower to a higher oxidation state [169]. Those oxides, which are characterized by a low transition enthalpy, form stable oxides and O_2 is not readily released. On the other hand, oxides with a very high transition enthalpy will not stabilize the OER intermediates. This explains the volcano-type dependence of the overpotential of the OER vs. the enthalpy change from lower to higher oxide (Fig. 24).

Along with the recent development of the regenerative fuel cells, interest in active catalysts for the OER has increased [170]. A regenerative fuel cell is a hydrogen–oxygen cell, which can operate both as a fuel cell and as an electrolyzer. When the cell works as an electrolyzer splitting water into H_2 and O_2, the hydrogen gas (and in some applications also the oxygen gas) is stored; on demand, electricity can then be generated from the stored H_2 through the fuel cell process. A regenerative fuel cell has a distinct advantage over state-of-the-art battery systems, because power and energy are separated: the energy is directly related to the fuel storage, whereas the rated power depends on the electrode area. This means that by simply increasing reactant storage, without changing the reactor stack(s), it is possible to increase the stored energy. Therefore, the mass advantage of typical advanced batteries loses out to that of regenerative fuel cells when the discharge time is increased beyond a few tens of minutes. Catalysts for the oxygen electrode of a regenerative fuel cell must therefore be active towards both oxygen evolution and oxygen reduction. One of the promising approaches in catalyst development relies on the combinatorial discovery of novel materials. Using this approach, Chen et al. [170] discovered a ternary $Pt_{4.5}Ru_4Ir_{0.5}$ catalyst with superior catalytic activity and stability. It was suggested that the addition of Ru to PtIr alloys increases the reaction rate by stabilizing M−O bonds and accelerating the oxidative deprotonation of M−OH groups.

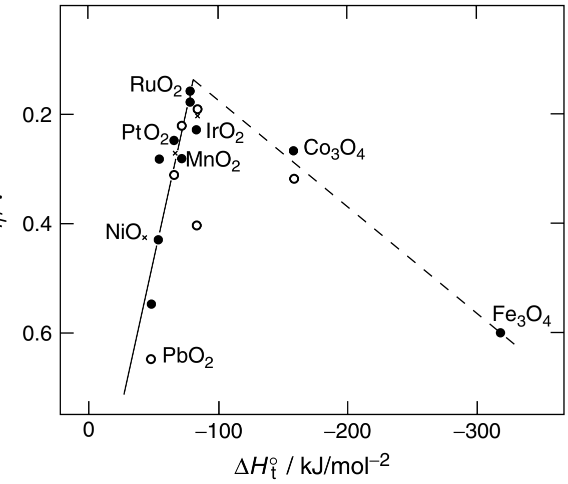

Fig. 24 Volcano plot of the overpotential for the OER versus the enthalpy of the lower to higher oxide transition. Open circles correspond to alkaline and closed circles to acidic electrolytes. Reproduced with permission from Ref. [169].

8.1.1.7 **Outlook**

This chapter has introduced some fundamental principles of electrocatalysis and discussed the electrocatalytic reactions that occur at hydrogen and oxygen electrodes in detail. In the first part, emphasis was put on those properties of the electrochemical environment that introduce a qualitative difference to heterogeneous reactions and also on the theoretical foundation of phenomenological approaches that are used in practice to judge the quality of an electrocatalytic material. The second part demonstrated the application of these methods and exemplified at the same time the large variety of experimental methods that are available to study the solid/liquid interface and the diversity of catalyst forms (ranging from single crystals to supported nanoparticles) and materials that may be used. Furthermore, emphasis was put to demonstrate parallels between heterogeneous catalysis and electrocatalysis.

The material covered here is just the tip of the iceberg of the vast field of electrocatalysis which has developed rapidly during recent decades. Along with the further development of *in situ* spectroscopic techniques that allow the electrode of the solid/liquid interface to be monitored in real time and the evolution of *ab initio* quantum mechanical calculations of the structure of the interface and the kinetics of complex interfacial reactions including adsorption, bond breaking and bond formation, the rapid progress is likely to continue in the following decades. Improvements in the temporal and

References see page 1902

spatial resolution of traditional methods (e.g. vibrational spectroscopic techniques) will go in parallel with the application of new techniques, in particular those based on synchrotron and neutron facilities, which might allow atomic and electronic structures to be monitored under real conditions. Hence an understanding of some electrocatalytic processes on the atomic and molecular level seems to be within reach.

During recent decades, electrocatalysis has moved from the investigation of polycrystalline electrodes to well-defined single crystals, thin films and supported metal particles. Until now the interest in Pt and its alloys has been overwhelming; however, emphasis nowadays is shifting towards complex materials, but also to Ib group metals and other non-noble metals. Inducing lattice strain by fabricating metal overlayers on foreign substrates has proven to be a powerful tool to produce materials with desired properties. Further progress in this direction is expected through concerted experimental and theoretical approaches. A better understanding of supported electrocatalysts requires the utilization of well-defined systems allowing control of the particle size, shape and interparticle separations. In this context, of particular interest is the development of templating and nanopatterning approaches. Further progress in practical applications requires the development of complex multifunctional materials which will comprise both metallic and molecular blocks.

The catalyst support is nowadays attracting increased attention and it is widely recognized that it affects all vital properties of electrocatalytic materials spanning from the intrinsic catalytic activity to macrokinetics. The range of materials which are utilized as electrocatalytic supports has expanded greatly recently and includes novel carbon materials, e.g. carbon nanotubes, nanofibers, mesoporous carbons with well-defined structures and non-carbonaceous supports, in particular metal oxides with semiconducting properties and electron-conducting polymer materials. A very promising direction is the preparation of catalytic supports with predefined properties in order to enhance metal utilization and catalyst performance in real devices, e.g. fuel cells. Thanks to the mentioned recent advancements, the development of novel catalysts for practical applications is at the edge of moving towards rational design rather than trial and error approaches.

The growing technological interest in fuel cells has already brought the catalytic and electrochemical communities closer together and this tendency will gather momentum. Although the evolution of fuel cells, both SOFC and PEMFC, has been really spectacular during recent decades, other applications of heterogeneous electrocatalysis, e.g. in electrosynthesis and the "electrochemical incineration" of organic and inorganic hazards, has lagged behind but will pick up speed in the coming years.

Acknowledgement

The authors would like to express their gratitude to G. Ertl, H. Gasteiger and R. Adzic for careful reading the manuscript and to R. Adzic, H. Gasteiger, B. Hayden, L. A. Kibler, N. M. Markovic and S. Trasatti for kindly offering figures for this chapter.

References

1. W. Vielstich, A. Lamm, H. A. Gasteiger (Eds.), *Handbook of Fuel Cells. Fundamentals, Technology and Applications, Vol. 2: Electrocatalysis*, Wiley, Chichester, 2003, 783 pp.
2. S. McIntosh, R. J. Gorte, *Chem. Rev.* **2004**, *104*, 4845.
3. C. Lamy, J.-M. Léger, S. Srinivasan, in *Modern Aspects of Electrochemistry*, Vol. 34, B. E. Conway, J. O. 'M. Bockris, R. E. White (Eds.), Kluwer/Plenum Press, New York, 2002, p. 53.
4. S. C. Thomas, X. M. Ren, S. Gottesfeld, P. Zelenay, *Electrochim. Acta* **2002**, *47*, 3741.
5. S. Wasmus, A. Kuver, *J. Electroanal. Chem.* **1999**, *461*, 14.
6. C. Lamy, A. Lima, V. LeRhun, F. Delime, C. Coutanceau, J. M. Léger, *J. Power Sources* **2002**, *105*, 283.
7. S. Trasatti, in *Interfacial Electrochemistry: Theory, Experiment and Applications*, A. Wieckowski (Ed.), Marcel Dekker, New York, 1999, p. 769.
8. A. T. Kuhn, (Ed.), *Industrial Electrochemical Processes*, Elsevier, **1971**, pp. 632.
9. J. G. daSilva, M. O. F. Goulart, M. Navarro, *Tetrahedron* **1999**, *55*, 7405.
10. S. Kaneco, K. Iiba, N. Hiei, K. Otha, T. Mizuno, T. Suzuki, *Electrochim. Acta* **1999**, *44*, 4701.
11. D. M. Kolb, *Angew. Chem. Int. Ed.* **2001**, *40*, 1162.
12. A. Wieckowski (Ed.), *Interfacial Electrochemistry: Theory, Experiment and Applications*, Marcel Dekker, New York, 1999, 996 pp.
13. N. M. Markovic, P. N. Ross, *Surf. Sci. Rep.* **2002**, *45*, 121.
14. H. E. Hoster, H. A. Gasteiger, in *Handbook of Fuel Cells. Fundamentals, Technology and Applications, Vol. 2. Electrocatalysis*, W. Vielstich, A. Lamm, H. A. Gasteiger (Eds.), Wiley, Chichester, 2003, p. 236.
15. A. J. Bard, M. Stratmann, P. R. Unwin (Eds.), *Instrumentation and Electroanalytical Chemistry. Encyclopedia of Electrochemistry*, Vol. 3, Wiley-VCH, New York, 2003, 689 pp.
16. M. J. Weaver, *Top. Catal.* **1999**, *8*, 65.
17. C. Korzeniewski, *Crit. Rev. Anal. Chem.* **1997**, *27*, 81.
18. A. Rodes, J. M. Perez, A. Aldaz, in *Handbook of Fuel Cells. Fundamentals, Technology and Applications, Vol. 2: Electrocatalysis*, W. Vielstich, A. Lamm, H. A. Gasteiger (Eds.), Wiley, Chichester, 2003, p. 191.
19. A. E. Russell, A. Rose, *Chem. Rev.* **2004**, *104*, 4613.
20. R. R. Adzic, X. Wang, B. M. Ocko, J. McBreen, in *Handbook of Fuel Cells. Fundamentals, Technology and Applications, Vol. 2: Electrocatalysis*, W. Vielstich, A. Lamm, H. A. Gasteiger (Eds.), Wiley, Chichester, 2003, p. 279.
21. N. J. Tao, C. Z. Li, H. X. He, *J. Electroanal. Chem.* **2000**, *492*, 81.
22. K. Itaya, *Prog. Surf. Sci.* **1998**, *58*, 121.

23. D. M. Kolb, *Electrochim. Acta* **2000**, *45*, 2387–2402.
24. B. Pettinger, C. Bilger, J. Lipkowski, W. Schmickler, in *Interfacial Electrochemistry: Theory, Experiment and Applications*, A. Wieckowski (Ed.), Marcel Dekker, New York, 1999, p. 373.
25. Y. Y. Tong, A. Wieckowski, E. Oldfield, *J. Phys. Chem. B* **2002**, *106*, 2434.
26. P. K. Babu, E. Oldfield, A. Wieckowski, in *Modern Aspects of Electrochemistry*, Vol. 36, C. G. Vayenas, B. E. Conway, R. E. White (Eds.), Kluwer/Plenum Press, New York, 2003, p. 1.
27. A. R. Hillman, in *Instrumentation and Electroanalytical Chemsitry. Encyclopedia of Electrochemistry*, Vol. 3, A. J. Bard, M. Stratmann, P. R. Unwin (Eds.), Wiley-VCH, Weinheim, 2003, p. 230.
28. R. M. Torresi, S. Wasmus, in *Handbook of Fuel Cells. Fundamentals, Technology and Applications*, Vol. 2, W. Vielstich, A. Lamm, H. A. Gasteiger (Eds.), Wiley, Chichester, 2003, p. 163.
29. A. Ignaczak, W. Schmickler, S. Bartenschlager, *J. Electroanal. Chem.* **2006**, *586*, 297.
30. E. Spohr, *Electrochim. Acta* **1999**, *44*, 1697.
31. P. Vassilev, R. A. v. Santen, M. T. M. Koper, *J. Chem. Phys.* **2005**, *122*, 1.
32. A. M. Kuznetsov, J. Ulstrup, *Electrochim. Acta* **2000**, *45*, 2339.
33. R. R. Nazmutdinov, G. A. Tsirlina, O. A. Petrii, Y. I. Kharkats, A. M. Kuznetsov, *Electrochim. Acta* **2000**, *45*, 3521.
34. E. D. German, A. M. Kuznetsov, M. Sheintuch, *Surf. Sci.* **2004**, *554*, 159.
35. B. P. Sullivan, K. Krist, H. E. Guard (Eds.), *Electrochemical and Electrocatalytic Reactions of Carbon Dioxide*, Elsevier, Amsterdam, 1993, 300 pp.
36. P. J. Gellings, H. J. M. Bouwmeester (Eds.), *The CRC Handbook of Solid State Electrochemistry*, CRC Press, Boca Raton, Fl, 1996, 630 pp.
37. S. J. C. Cleghorn, X. Ren, T. E. Springer, M. S. Wilson, C. Zawodizinski, T. A. Zawodzinski, S. Gottesfeld, *Int. J. Hydrogen Energy* **1997**, *22*, 1137.
38. K. Uosaki, H. Kita, in *Modern Aspects of Electrochemistry*, Vol. 18, R. E. White, J. O. 'M. Bockris, B. E. Conway (Eds.), Plenum Press, New York, 1986.
39. Note that this applies to metal electrodes; in the case of semiconductor electrodes, the interfacial region propagates much deeper into the bulk of the electrode.
40. A. J. Bard, L. R. Faulkner, *Electrochemical Methods*, Wiley-VCH, Weinheim, 2001, 833 pp.
41. Note that in this section, all energetic quantities refer to a single particle; in a chemical context, molar quantities are more common. To convert particle energies to molar energies they have to be multiplied by Avogadro's number.
42. The thus defined potential of zero charge corresponds to the so-called potential of zero free charge, to be distinguished from the potential of zero total charge; for details, see A. Frumkin, O. A. Petrii, B. Damaskin, in *Comprehensive Treatise of Electrochemistry*, J. O. 'M. Bockris, B. E. Conway, E. Yeager (Eds.), Plenum Press, New York, 1980, p. 201.
43. J. O. 'M. Bockris, S. U. M. Khan, *Surface Electrochemistry*, Plenum Press, New York, 1993, 1046 pp.
44. Note that above we considered only equilibrium conditions and thus E denoted the equilibrium potential, which from now on we denote by E^{eq}.
45. In an outer-sphere charge transfer, an electron is transferred between two species or between an electrode and a species without participation of the coordination sphere of the species, i.e. the latter is maintained. Correspondingly, in an inner sphere charge transfer reaction the coordination shell takes part.
46. R. A. Marcus, *Angew. Chem. Int. Ed.* **1992**, *32*, 1111.
47. N. S. Hush, *J. Electroanal. Chem.* **1999**, *470*, 170.
48. A. M. Kuznetsov, in *Modern Aspects of Electrochemistry*, Vol. 20, R. E. White, J. O. 'M. Bockris, B. E. Conway (Eds.), Plenum Press, New York, 1989, p. 95.
49. A. M. Kuznetsov, J. Ulstrup, *Electron Transfer in Chemistry and Biology: an Introduction to Theory*, Wiley, Chichester, 1999, 358 pp.
50. R. J. D. Miller, G. L. McLendon, A. J. Nozik, W. Schmickler, F. Willig, *Surface Electron Transfer Processes*, VCH, New York, 1995, 370 pp.
51. M. J. Weaver, in *Comprehensive Chemical Kinetics*, Vol. 27, R. G. Compton (Ed.), Elsevier, Amsterdam, 1987, Ch. 1.
52. A. M. Kuznetsov, J. Ulstrup, *Electrochim. Acta* **2000**, *45*, 2339.
53. E. D. German, A. M. Kuznetsov, M. Sheintuch, *Surf. Sci.* **2004**, *554*, 159.
54. Note that in this chapter G always denotes the standard free energy, which is conventionally denoted by G^0, to avoid an extensive number of super- and subscripts.
55. In the electrochemical literature, the Butler–Volmer equation is given usually for an n-electron transfer reaction, in which case the exponents are multiplied by n. It is questionable, however, whether single-step reactions with an n-electron transfer exist.
56. J. O. 'M. Bockris, A. K. N. Reddy, M. Gamboa-Aldeco, *Modern Electrochemistry 2A: Fundamentals of Electronics*, 2nd Ed., Kluwer/Plenum Press, New York, 2000, 1534 pp.
57. D. K. Lambert, *Electrochim. Acta* **1996**, *41*, 623.
58. J. K. Sass, K. Bange, *ACS Symp. Ser.* **1988**, *378*, 54.
59. F. T. Wagner, in *Structure of Electrified Interfaces*, J. Lipkowski, P. N. Ross (Eds.), VCH, New York, 1993, p. 309.
60. W. Nicholson, A. Carlisle, *Nicholson's J.* **1800**, *4*, 183.
61. J. Tafel, *Z. Phys. Chem.* **1905**, *50*, 641.
62. N. I. Kobosev, N. I. Nekrasova, *Z. Elektrochem.* **1930**, *36*, 68.
63. N. I. Kobosev, V. V. Monblanova, *Zh. Fiz. Khim.* **1936**, *7*, 645.
64. A. N. Frumkin, in *Advances in Electrochemistry and Electrochemical Engineering*, P. Delahay, C. W. Tobias (Eds.), Interscience, New York, 1961, p. 65.
65. A. N. Frumkin, in *Advances in Electrochemistry and Electrochemical Engineering*, P. Delahay, C. W. Tobias (Eds.), Interscience, New York, 1963, p. 287.
66. M. W. Breiter, in *Handbook of Fuel Cells: Fundamentals, Technology and Applications, Vol. 2: Electrocatalysis*, Wiley, Chichester, 2003, p. 361.
67. N. M. Markovic, in *Handbook of Fuel Cells: Fundamentals, Technology and Applications, Vol. 2: Electrocatalysis*, Wiley, Chichester, 2003, p. 368.
68. A. Lasia, in *Handbook of Fuel Cells: Fundamentals, Technology and Applications, Vol. 2: Electrocatalysis*, Wiley, Chichester, 2003, p. 416.
69. B. E. Conway, in *Interfacial Electrochemistry. Theory, Experiment and Applications*, A. Wieckowski (Ed.), Marcel Dekker, New York, 1999, p. 131.
70. G. Jerkiewicz, *J. Electrochem. Soc.* **1996**, *143*, 1240.
71. G. Jerkiewicz, *Prog. Surf. Sci.* **1998**, *57*, 137.
72. O. A. Petrii, G. A. Tsirlina, *Electrochim. Acta* **1994**, *39*, 1739.
73. K. J. Vetter, *Elektrochemische Kinetik*, Springer-Verlag, Berlin, 1961, 698 pp.
74. M. Temkin, *Zh. Fiz. Khim.* **1941**, *15*, 296.
75. A. N. Frumkin, *Z. Phys.* **1926**, *35*, 792.
76. M. Breiter, R. Clamroth, *Z. Elektrochem.* **1954**, *58*, 1954.
77. J. O. 'M. Bockris, *Trans. Faraday Soc.* **1947**, *43*, 417.

78. S. Trasatti, *J. Electroanal. Chem.* **1971**, *33*, 351.
79. S. Trasatti, *J. Electroanal. Chem.* **1972**, *39*, 163.
80. B. E. Conway, J. O. 'M. Bockris, *J. Chem. Phys.* **1957**, *26*, 532.
81. R. Parsons, *Trans. Faraday Soc.* **1958**, *34*, 1053.
82. L. I. Krishtalik, in *Advances in Electrochemistry and Electrochemical Engineering*, Vol. 7, P. Delahay (Ed.), Interscience, New York, 1970.
83. B. E. Conway, B. V. Tilak, *Electrochim. Acta* **2002**, *47*, 3571.
84. N. M. Markovic, B. N. Grgur, P. N. Ross, *J. Phys. Chem. B* **1997**, *101*, 5405.
85. N. M. Markovic, S. T. Sarraf, H. A. Gasteiger, P. N. Ross, *J. Chem. Soc., Faraday Trans.* **1996**, *92*, 3719.
86. T. R. Ralph, M. P. Hogarth, *Platinum Met. Rev.* **2002**, *46*, 117.
87. A. N. Frumkin, B. Slygin, *Acta Physicochim. URSS* **1935**, *3*, 791.
88. J. Clavilier, *J. Electroanal. Chem.* **1980**, *107*, 211.
89. C. Lamy, J. M. Leger, J. Clavilier, *J. Electroanal. Chem.* **1982**, *135*, 321.
90. A. T. Gee, B. E. Hayden, C. Mormiche, T. S. Nunney, *J. Chem. Phys.* **2000**, *112*, 7660.
91. S. M. Davis, G. A. Somorjai, *Surf. Sci.* **1985**, *161*, 597.
92. K. Christmann, *Surf. Sci. Rep.* **1988**, *9*, 1.
93. P. N. Ross, *Surf. Sci.* **1981**, *102*, 463.
94. A. Zolfaghari, G. Jerkiewicz, *J. Electroanal. Chem.* **1999**, *467*, 177.
95. N. M. Markovic, T. J. Schmidt, B. N. Grgur, H. A. Gasteiger, R. J. Behm, P. N. Ross, *J. Phys. Chem. B* **1999**, *103*, 8568.
96. M. T. M. Koper, R. A. van Santen, *J. Electroanal. Chem.* **1999**, *472*, 126.
97. D. E. Ramaker, M. Teliska, Y. Zhang, A. Y. Stakheev, D. C. Koningsberger, *Phys. Chem. Chem. Phys.* **2003**, *5*, 4492.
98. A. Kolics, A. Wieckowski, *J. Phys. Chem. B* **2001**, *105*, 2588.
99. B. Hammer, J. K. Nørskov, *Surf. Sci.* **1995**, *343*, 211.
100. A. Ruban, B. Hammer, P. Stoltze, H. L. Skriver, J. K. Nørskov, *J. Mol. Catal. A* **1997**, *115*, 421.
101. L. A. Kibler, A. M. El-Aziz, R. Hoyer, D. M. Kolb, *Angew. Chem. Int. Ed.* **2005**, *44*, 2080.
102. B. E. Conway, *Sci. Prog., Oxf.* **1987**, *71*, 479.
103. B. E. Conway, G. Jerkiewicz, *Electrochim. Acta* **2000**, *45*, 4075.
104. K. Kunimatsu, H. Uchida, M. Osawa, M. Watanabe, *J. Electroanal. Chem.* **2006**, *587*, 299.
105. A. Peremans, A. Tadjeddine, *Phys. Rev. Lett.* **1994**, *73*, 3010.
106. A. Tadjeddine, A. Peremans, *Surf. Sci.* **1996**, *368*, 377.
107. M. Teliska, W. E. O'Grady, D. E. Ramaker, *J. Phys. Chem. B* **2004**, *108*, 2333.
108. M. R. Tarasevich, A. Sadkowski, E. Yeager, in *Comprehensive Treatise of Electrochemistry*, Vol. 7, B. E. Conway, J. O. 'M. Bockris, E. Yeager, S. U. M. Khan, R. E. White (Eds.), Plenum Press, New York, 1983, p. 301.
109. A. Damjanovic, in *Electrochemistry in Transition*, O. J. Murphy, S. Srinivasan, B. E. Conway (Eds.), Plenum Press, New York, 1992, p. 107.
110. K. Kinoshita, *Electrochemical Oxygen Technology*, Wiley, New York, 1992, 448 pp.
111. R. Adzic, in *Electrocatalysis*, J. Lipkowski, P. N. Ross (Eds.), Wiley-VCH, New York, 1998, p. 197.
112. G. Gattrell, B. MacDougall, in *Handbook of Fuel Cells. Fundamentals, Technology, Applications, Vol. 2: Electrocatalysis*, W. Vielstich, A. Lamm, H. A. Gasteiger (Eds.), Wiley, New York, 2003, p. 444.
113. S. B. Adler, *Chem. Rev.* **2004**, *104*, 4791.
114. H. Wroblowa, Y. C. Pan, J. Razumney, *J. Electroanal. Chem.* **1976**, *69*, 195.
115. V. S. Bagotskii, M. R. Tarasevich, V. Y. Filinovskii, *Elektrokhimiya* **1969**, *5*, 1218.
116. A. Frumkin, L. Nekrasov, B. Levich, J. Ivanov, *J. Electroanal. Chem.* **1959**, *1*, 85.
117. R. R. Adzic, S. Strbac, N. Anastasijevic, *Mater. Chem. Phys.* **1989**, *22*, 349.
118. B. E. Conway, *Prog. Surf. Sci.* **1995**, *49*, 331.
119. G. Jerkiewicz, in *Interfacial Electrochemistry*, A. Wieckowski (Ed.), Marcel Dekker, New York, 1999, p. 559.
120. A. Chen, J. Lipkowski, *J. Phys. Chem. B* **1999**, *103*, 682.
121. E. R. Savinova, A. Scheybal, M. Danckwerts, U. Wild, B. Pettinger, K. Doblhofer, R. Schlogl, G. Ertl, *Faraday Discuss.* **2002**, *121*, 181.
122. S. L. Horswell, A. L. N. Pinheiro, E. R. Savinova, M. Danckwerts, B. Pettinger, M. S. Zei, G. Ertl, *Langmuir* **2004**, *20*, 10970.
123. A. B. Anderson, *Electrochim. Acta* **2002**, *47*, 3759.
124. Y. Zhang, X. Gao, M. J. Weaver, *J. Phys. Chem.* **1993**, *97*, 8656.
125. E. R. Savinova, P. Kraft, B. Pettinger, K. Doblhofer, *J. Electroanal. Chem.* **1997**, *430*, 47.
126. G. C. Allen, P. M. Tucker, A. Capon, R. Parsons, *J. Electroanal. Chem.* **1974**, *50*, 335.
127. D. Hecht, P. Borthen, H.-H. Strehblow, *Surf. Sci.* **1996**, *365*, 263.
128. B. Cabrera, N. F. Mott, *Rep. Prog. Phys.* **1949**, *12*, 163.
129. V. I. Birss, M. Chang, J. Segal, *J. Electroanal. Chem.* **1993**, *355*, 181.
130. G. Jerkiewicz, G. Vatankhah, J. Lessard, M. P. Soriaga, Y.-S. Park, *Electrochim. Acta* **2004**, *49*, 1451.
131. H. Y. H. Chan, S. Zou, M. J. Weaver, *J. Phys. Chem. B* **1999**, *103*, 11141.
132. Although the wavenumber is in good accord with that for Pt–O in PtO_2, a shift was observed when H_2O was replaced by D_2O, somewhat questioning the band attribution.
133. P. G. Allen, S. D. Conradson, M. S. Wilson, S. Gottesfeld, I. D. Raistrick, J. Valerio, M. Lovato, *J. Electroanal. Chem.* **1995**, *384*, 99.
134. A. Damjanovic, V. Brusic, *Electrochim. Acta* **1967**, *12*, 615.
135. V. S. Murthi, R. C. Urian, S. Mukerjee, *J. Phys. Chem. B* **2004**, *108*, 11011.
136. E. Yeager, *J. Mol. Catal.* **1986**, *38*, 5.
137. J. S. Griffith, *Proc. R. Soc. London, Ser. A* **1956**, *235*, 23.
138. L. Pauling, *Nature* **1964**, *203*, 182.
139. R. R. Adzic, J. X. Wang, *J. Phys. Chem. B* **1998**, *102*, 8988.
140. R. A. Sidik, A. B. Anderson, *J. Electroanal. Chem.* **2002**, *528*, 69.
141. A. B. Anderson, T. V. Albu, *Electrochem. Commun.* **1999**, *1*, 203.
142. J. K. Nørskov, J. Rossmeisl, A. Logadottir, L. Lindqvist, J. R. Kitchin, T. Bligaard, H. Jonsson, *J. Phys. Chem. B* **2004** *108*, 17886.
143. J. L. Zhang, M. B. Vukmirovic, Y. Xu, M. Mavrikakis, R. R. Adzic, *Angew. Chem. Int. Ed.* **2005**, *44*, 2132.
144. T. Li, P. B. Balbuena, *J. Phys. Chem. B* **2001**, *105*, 9943.
145. T. Li, P. B. Balbuena, *Chem. Phys. Lett.* **2003**, *367*, 439.
146. A. Panchenko, M. T. M. Koper, T. E. Shubina, S. J. Mitchell, E. Roduner, *J. Electrochem. Soc.* **2004**, *151*, A2016.
147. P. B. Balbuena, D. Altomare, L. Agapito, J. M. Seminario, *J. Phys. Chem. B* **2003**, *107*, 13671.

148. A. B. Anderson, T. V. Albu, *J. Electrochem. Soc.* **2000**, *147*, 4229.
149. A. B. Anderson, J. Roques, S. Mukerjee, V. S. Murthi, N. M. Markovic, V. Stamenkovic, *J. Phys. Chem. B* **2005**, *109*, 1198.
150. B. N. Grgur, N. M. Markovic, P. N. Ross, *Can. J. Chem. - Rev. Can. Chim* **1997**, *75*, 1465.
151. K. Kinoshita, *Carbon: Electrochemical and Physicochemical Properties*, Wiley, New York, 1988, 533 pp.
152. A. V. Dribinskii, M. R. Tarasevich, V. E. Kazarinov, *Mater. Chem. Phys.* **1989**, *22*, 377.
153. T. J. Schmidt, V. Stamenkovic, P. N. Ross, N. M. Markovic, *Phys. Chem. Chem. Phys.* **2003**, *5*, 400.
154. J. X. Wang, N. M. Markovic, R. R. Adzic, *J. Phys. Chem. B* **2004**, *108*, 4127.
155. D. Thompsett, in *Handbook of Fuel Cells: Fundamentals, Technology and Applications*, Vol. 3, W. Vielstich, H. Gasteiger, A. Lamm (Eds.), Wiley, Chichester, 2003, p. 467.
156. H. A. Gasteiger, S. S. Kocha, B. Sompalli, F. T. Wagner, *Appl. Catal. B* **2005**, *56*, 9.
157. K. Kinoshita, *J. Electrochem. Soc.* **1990**, *137*, 845.
158. K. Kinoshita, in *Modern Aspects of Electrochemistry*, Vol. 14, J. O. 'M. Bockris, B. E. Conway, R. E. White (Eds.), Plenum Press, New York, 1982, p. 557.
159. S. Mukerjee, in *Catalysis and Electrocatalysis at Nanoparticle Surfaces*, A. Wieckowski, E. R. Savinova, C. G. Vayenas (Eds.), Marcel Dekker, New York, 2003, p. 501.
160. N. M. Markovic, T. J. Schmidt, V. Stamenkovic, P. N. Ross, *Fuel Cells* **2001**, *105–116*.
161. Y. Xu, A. V. Ruban, M. Mavrikakis, *J. Am. Chem. Soc.* **2004**, *126*, 4717.
162. S. R. Brankovic, J. X. Wang, R. R. Adzic, *Electrochem. Solid State Lett.* **2001**, *4*, A217.
163. R. R. Adzic, in *Encyclopedia of Electrochemistry*, Vol. 1, A. J. Bard, M. Stratmann (Eds.), Wiley-VCH, New York, 2002, p. 561.
164. M. Mavrikakis, B. Hammer, J. K. Nørskov, *Phys. Rev. Lett.* **1998**, *81*, 2819.
165. J. B. Goodenough, B. L. Cushing, in *Handbook of Fuel Cells. Fundamentals, Technology and Applications, Vol. 2: Electrocatalysis*, W. Vielstich, A. Lamm, H. A. Gasteiger (Eds.), Wiley, Chichester, 2003, p. 521.
166. J. H. Zagal, in *Handbook of Fuel Cells. Fundamentals, Technology and Applications, Vol. 2: Electrocatalysis*, W. Vielstich, A. Lamm, H. A. Gasteiger (Eds.), Wiley, Chichester, 2003, p. 544.
167. N. Alonso-Vante, in *Handbook of Fuel Cells. Fundamentals, Technology and Applications, Vol. 2: Electrocatalysis*, W. Vielstich, A. Lamm, H. A. Gasteiger (Eds.), Wiley, Chichester, 2003, p. 534.
168. K. I. Rosenthal, V. I. Veselovski, *Dokl. Akad. Nauk SSSR* **1956**, *111*, 637.
169. S. Trasatti, *Electrochim. Acta* **1984**, *29*, 1503.
170. G. Chen, D. A. Delafuente, S. Sarangapani, T. E. Mallouk, *Catal. Today* **2001**, *67*, 341.
171. B. E. Hayden, in *Catalysis and Electrocatalysis at Nanoparticle Surfaces*, A. Wieckowski, E. R. Savinova, C. G. Vayenas (Eds.), Marcel Dekker, New York, 2003, p. 171.
172. N. M. Markovic, H. A. Gasteiger, N. Philip, *J. Phys. Chem.* **1996**, *100*, 6715.

8.1.2
Electrochemical Modification of Catalytic Activity

Constantinos G. Vayenas, Alexandros Katsaounis, Susanne Brosda, and Ahmad Hammad*

8.1.2.1 Introduction

8.1.2.1.1 Catalytic and Electrocatalytic Kinetics Heterogeneous catalysis and aqueous or solid electrochemistry have been treated traditionally as different branches of physical chemistry, yet similar concepts are used to model their kinetics [1–4] and similar surface science techniques are used to investigate their fundamental aspects at the molecular level [1–8]. The growing technological interest in fuel cells, both high-temperature solid oxide fuel cells (SOFCs) and low-temperature polymeric electrolyte membrane (PEM) fuel cells, has brought the catalytic and electrochemical communities closer, as the merits of catalysis in designing and operating efficient anodes and cathodes is being more widely recognized [9–11].

An important additional operating parameter in electrochemical (electrocatalytic, i.e. net charge transfer) vs. catalytic (no net charge transfer) kinetics is the electrical potential dependence of the electrochemical rate, yet in recent years its has been shown that for electrochemically promoted catalysts (i.e. catalysts in contact with a solid electrolyte [12–18]) the *catalytic* rate also depends dramatically on catalyst potential, similarly to the electrochemical rate.

It has been known for some years that electrochemistry can be used to activate and tune precisely heterogeneous catalytic processes when the catalyst is in contact with ionic or mixed ionic–electronic conductors as supports (e.g. YSZ, TiO_2, CeO_2) [12–39]. These materials act as specific anionic or cationic conductors and, depending on their composition, have catalytically useful electrical conductivities at temperatures of 25–1000 °C. Within this temperature range, which covers practically all heterogeneous catalytic reactions, solid electrolytes can be used as reversible *in situ promoter donors* and/or poison acceptors to affect the catalytic activity and selectivity of metals deposited on solid electrolytes in a very pronounced, reversible and, to some extent, predictable manner. This is accomplished by applying a potential (±1–2 V) between the conductive catalyst film and a second metal film (counter electrode) also interfaced with the solid electrolyte and thus causing a controlled migration (backspillover) of promoting ions from the solid electrolyte on to the catalyst surface.

References see page 1934

* Corresponding author.